Optical and Quantum Electronics 9 (1977) 315–349

Generation of picosecond light continua by parametric four-photon interactions in liquids and solids

A. PENZKOFER, W. KAISER
Physik-Department der Technischen Universität München, Germany

Received 20 December 1976

Light continua extending from the i.r. to the u.v. are generated with picosecond laser pulses in liquids and solids. It is demonstrated that the light spectra in water are produced by stimulated parametric four-photon interactions, which are resonantly enhanced by single and difference frequency resonances of the non-linear susceptibility $\chi^{(3)}$. A theory of the various parametric four-photon interaction processes is developed and the resonant structure of $\chi^{(3)}$ is discussed. The experimental results are compared with theoretical calculations. The generation of light continua by other nonlinear optical processes is briefly discussed.

1. Introduction

During the past years spectral super-broadening of picosecond light pulses in liquids and glasses has been reported by several authors [1–8]. In most experiments the broad frequency spectra were generated in the presence of self-focusing of the laser beam [1–6]. Homogeneous spectral distributions were found in different materials. Typical values for the broadening were several thousand wave-numbers on both sides of the laser frequency. The duration of the spectra was found to be nearly the same as the duration of the laser pulse [4, 6, 8]. The generated spectra were emitted in the forward direction and had the same polarization as the laser light [4, 8]. In early papers [1–5] the main mechanism responsible for the super-broadening of picosecond light pulses was thought to be self-phase modulation. Calculations show that very high peak intensities and very short pulse durations are necessary for substantial spectral broadening by self-phase modulation. In addition to the broad radiation emitted in the forward direction, a continuous spectrum was found to be emitted under a certain angle [2]. In this case a glass sample was used and light intensities of $I_L \simeq 10^{13}\,\mathrm{W/cm^2}$ were reported. The cone shaped spectrum was explained by phase-matched parametric four-photon interaction. In another paper [9] a periodic structure has been observed in the forward emitted spectrum when self-focusing of single picosecond light pulses in glasses occurred. A four-photon parametric process was thought to be responsible for the modulation.

In our experiments we studied the generation of light spectra under well-defined conditions [8]. The complex situation of self-focusing of the laser beam did not occur in our investigations. This fact made it possible to study the build-up of the spectrum with increasing intensity. The generated radiation started at discrete frequencies away from the laser frequency. It increased approximately exponentially with increasing laser intensity until saturation occurred. It broadened and extended over a wide spectral range with increasing intensity. Our experimental results can be explained by stimulated parametric four-photon processes. These processes occur in water despite large phase-mismatch and large infrared absorption because of the resonant structure of the nonlinear susceptibility $\chi^{(3)}$ and the high laser intensity.

Picosecond light continua represent ideal light sources for ultrashort time-resolved spectroscopy. Broad light spectra have been applied in a variety of investigations, e.g. photo-bleaching [6, 10] and

excited-state absorption [11], electron solvent interaction [12], exciton formation in crystals [13, 14], and two-photon absorption spectroscopy [15].

The great importance of picosecond continua as light sources for picosecond spectroscopy justifies a detailed study of their generation and their properties.

In Section 2 the theory of four-photon interaction is presented. It includes four-photon parametric interaction, four-photon frequency conversion, three-frequency mixing and third harmonic generation. The finite band-width of the pump pulses, the phase-mismatch and the linear absorption losses are taken into account.

In Section 3 the frequency dependence of the nonlinear susceptibility $\chi^{(3)}$ is discussed in some detail. The resonant structure of $\chi^{(3)}$ is of vital importance for the understanding of the generation of the broad spectra. $\chi^{(3)}$ will be separated into three parts, a non-resonant part, a part containing single frequency resonances and a part containing double (difference) frequency resonances. The single frequency resonances are related to infrared absorption while double frequency resonances are connected to the Raman susceptibility.

In Section 4 the experimental system is described. Single picosecond pulses from a mode-locked Nd-glass laser were used to generate picosecond pulses at new frequencies. Most investigations were made with liquid water as sample material.

In Section 5 we present our experimental results. Light spectra ranging from the infrared to the ultraviolet region are observed and analysed. The intensity dependence of the spectral build-up is studied. It is shown that parametric four-photon processes, frequency conversion processes, three-frequency mixing, and third harmonic generation are involved in the generation of the picosecond spectra. Data on conversion efficiencies are reported.

In Section 6 other nonlinear processes leading to broad frequency spectra are investigated. The effects of self-phase modulation due to the intensity dependence of the refractive index, due to heating of the sample and due to plasma formation are discussed. The influence of stimulated Raman scattering on parametric light generation is considered. The complex situation in the case of self-focusing is emphasized.

2. Theory

2.1. General equations

Intense laser light induces a nonlinear polarization which gives rise to various nonlinear optical effects [16–22]. When the induced polarization is expanded in a power series, we obtain a nonlinear term proportional to the third power of the electric field

$$P_{\mathrm{NL}}^{(3)} = \chi_0^{(3)} EEE \tag{1}$$

This term is the lowest order nonlinear term in materials with an inversion centre. The polarization $P_{\mathrm{NL}}^{(3)}$ leads to a variety of physical phenomena [16–22]. Here we are concerned with parametric four-photon generation of new light frequencies.

In our calculations we write the electric field strength $E_x(z, t) = E(z, t)$, $E_y = 0$, $E_z = 0$ and the nonlinear polarization as follows:

$$E(t, z) = \frac{1}{2\pi} \int_{-\infty}^{+\infty} E(\omega, z) \exp(i\omega t)\, \mathrm{d}\omega \tag{2}$$

and [18–20]

$$P_{\mathrm{NL},i}^{(3)}(t, z) = \frac{1}{2\pi} \int_{-\infty}^{\infty} P_{\mathrm{NL},i}^{(3)}(\omega, z) \exp(i\omega t)\, \mathrm{d}\omega \tag{3a}$$

$$= \frac{1}{8\pi^3} \int_{-\infty}^{\infty} \mathrm{d}\omega_\alpha \int_{-\infty}^{\infty} \mathrm{d}\omega_\beta \int_{-\infty}^{\infty} \mathrm{d}\omega_\gamma \chi_{i,xxx}^{(3)}(\omega_\alpha, \omega_\beta, \omega_\gamma)$$

$$\times E(\omega_\alpha, z) E(\omega_\beta, z) E(\omega_\gamma, z) \exp[i(\omega_\alpha + \omega_\beta + \omega_\gamma)t] \tag{3b}$$

$$= \frac{1}{8\pi^3} \int_{-\infty}^{\infty} \mathrm{d}\omega \int_{-\infty}^{\infty} \mathrm{d}\omega_\alpha \int_{-\infty}^{\infty} \mathrm{d}\omega_\beta \int_{-\infty}^{\infty} \mathrm{d}\omega_\gamma \delta(-\omega + \omega_\alpha + \omega_\beta + \omega_\gamma)$$

$$\times \chi^{(3)}_{i,xxx}(-\omega;\omega_\alpha,\omega_\beta,\omega_\gamma)E(\omega_\alpha,z)E(\omega_\beta,z)E(\omega_\gamma,z)\exp(i\omega t) \tag{3c}$$

We follow the notation of [18, 19], $\chi^{(3)} = 0.25\chi^{(3)}_0$; i stands for x, y, or z and $E(-\omega_\nu, z) = E^*(\omega_\nu, z)$. The nonlinear susceptibility $\chi^{(3)}$ represents a fourth rank tensor.

In the case of linearly polarized light, the interaction between light and matter is described by the wave equation

$$\frac{\partial^2 E}{\partial z^2} - \frac{n^2}{c^2}\frac{\partial^2 E}{\partial t^2} - \frac{\alpha n}{c}\frac{\partial E}{\partial t} = \frac{4\pi}{c^2}\frac{\partial^2 P^{(3)}_{NL}}{\partial t^2}. \tag{4}$$

We introduce the values for $E(t, z)$ and $P^{(3)}_{NL}(t, z)$ from Equations 2 and 3c, respectively and make the substitution $E(\omega_\nu, z) = E_0(\omega_\nu, z) \times \exp(-ik_\nu z)$. When Fourier components of equal frequency are equated, one obtains for the frequency component ω

$$\frac{\partial E_0(\omega)}{\partial z} = -\frac{\alpha}{2}E_0(\omega) - \frac{i\omega}{2\pi cn}\int_{-\infty}^{\infty} d\omega_\alpha \int_{-\infty}^{\infty} d\omega_\beta \chi^{(3)}_{xxxx}(-\omega;\omega_\alpha,\omega_\beta,\omega_\gamma)E_0(\omega_\alpha)E_0(\omega_\beta)E_0(\omega_\gamma)\exp(i\Delta kz) \tag{5}$$

where $\omega = \omega_\alpha + \omega_\beta + \omega_\gamma$ and $\Delta k = k - k_\alpha - k_\beta - k_\gamma$. The approximations $\partial^2 E_0(\omega)/\partial z^2 \ll k^2 E_0(\omega)$ and the relation $k^2 - n^2\omega^2/c^2 = 0$ were used. The first term on the right hand side results from the linear losses at frequency ω. The second term gives the interaction of the field at frequency ω with the other frequency components. Note, that Equation 5 represents an infinite number of coupled equations.

In the following we consider the case where the band widths $\Delta\omega_\alpha$ and $\Delta\omega_\beta$ of the electric fields $E(\omega_\alpha)$ and $E(\omega_\beta)$ are small. The variations of the nonlinear susceptibility $\chi^{(3)}_{xxxx}(-\omega;\omega_\alpha,\omega_\beta,\omega_\gamma)$, of the phase mismatch Δk, and of the field $E_0(\omega_\gamma)$ are neglected within the small frequency intervals

$$\bar{\omega}_\alpha - \Delta\omega_\alpha/2 \leqslant \omega_\alpha \leqslant \bar{\omega}_\alpha + \Delta\omega_\alpha/2,$$

$$\bar{\omega}_\beta - \Delta\omega_\beta/2 \leqslant \omega_\beta \leqslant \bar{\omega}_\beta + \Delta\omega_\beta/2$$

and

$$\bar{\omega}_\gamma - (\Delta\omega_\alpha + \Delta\omega_\beta)/2 \leqslant \omega_\gamma \leqslant \bar{\omega}_\gamma + (\Delta\omega_\alpha + \Delta\omega_\beta)/2,$$

where

$$\bar{\omega}_\gamma = \omega - \bar{\omega}_\alpha - \bar{\omega}_\beta.$$

$E_0(\omega)$, $E_0(\omega_\gamma)$, α, Δk and $\chi^{(3)}$ are now average values within these frequency intervals and when the integrations over ω_α and ω_β are carried out, Equation 5 reduces to

$$\frac{\partial E_0(\omega)}{\partial z} = -\frac{\alpha}{2}E_0(\omega) - \frac{i\omega}{2\pi nc}\chi^{(3)}_{xxxx}(-\omega,\bar{\omega}_\alpha,\bar{\omega}_\beta,\omega_\gamma)E_0(\omega_\gamma)\exp(i\Delta kz)\int_{-\infty}^{\infty} d\omega_\alpha E_0(\omega_\alpha)\int_{-\infty}^{\infty} d\omega_\beta E_0(\omega_\beta) \tag{6}$$

$$= -\frac{\alpha}{2}E_0(\omega) - \frac{i2\pi\omega}{nc}\chi^{(3)}_{xxxx}(-\omega,\bar{\omega}_\alpha,\bar{\omega}_\beta,\bar{\omega}_\gamma)E_{0\alpha}E_{0\beta}E_0(\omega_\gamma)\exp(i\Delta kz). \tag{7}$$

$E_{0\nu} = E_{0\nu}(t' = t - nz/c, z) = 1/(2\pi)\int_{-\infty}^{\infty} E_0(\omega_\nu, z)\, d\omega_\nu$ is the peak amplitude of the electric field with carrier frequency $\bar{\omega}_\nu$, i.e. $E_\nu(t', z) = E_{0\nu}(t', z)\cos(\bar{\omega}_\nu t - k_\nu z)$.

The condition that $\chi^{(3)}_{xxxx}(-\omega;\omega_\alpha,\omega_\beta,\omega_\gamma)$ changes only slightly within the bandwidths $\Delta\omega_\alpha$ and $\Delta\omega_\beta$ is fulfilled outside resonances. In our experimental studies on water, the condition is obeyed even around resonances (see below, Fig. 10) and Equations 7 are valid.

To solve Equations 7 the physical conditions have to be specified. We consider four cases: parametric four-photon interaction, four-photon frequency conversion, three-frequency mixing, and third harmonic generation.

2.2. Parametric four-photon interaction $\omega_1 + \omega_2 \rightarrow \omega_3 + \omega_4$.

2.2.1. Small signal approximation

Two strong pulses (pump pulses) at frequencies ω_1 and ω_2 (width $\Delta\omega_1$ and $\Delta\omega_2$; the special case $\omega_1 = \omega_2 = \omega_L$ is included) enter the medium. The light emitted at the signal frequency $\omega_3 =$

$\omega_1 + \omega_2 - \omega_4$ and at the idler frequency ω_4 is calculated ($\omega_\alpha = \omega_1, \omega_\beta = \omega_2, \omega_\gamma = -\omega_4, \omega = \omega_3$). The conversion of light from the pump waves to the signal and idler wave should be small, i.e. depletion of the pump pulse may be neglected (parametric approximation). Without linear absorption of the pump waves ($\alpha_1 = \alpha_2 = 0$) Equation 7 reduces to a set of two coupled differential equations.

$$\frac{\partial E_0(\omega_3)}{\partial z} = -\frac{\alpha_3}{2}E_0(\omega_3) - \frac{i2\pi\omega_3}{n_3 c}\chi^{(3)}_{xxxx}(-\omega_3;\omega_1,\omega_2,-\omega_4)E_0^*(\omega_4)E_{01}E_{02}\exp(i\Delta kz) \tag{8a}$$

$$\frac{\partial E_0^*(\omega_4)}{\partial z} = -\frac{\alpha_4}{2}E_0^*(\omega_4) + \frac{i2\pi\omega_4}{n_4 c}\chi^{(3)*}_{xxxx}(-\omega_4;\omega_1,\omega_2,-\omega_3)E_0(\omega_3)E_{01}^*E_{02}^*\exp(-i\Delta kz). \tag{8b}$$

It will be shown below that $\chi^{(3)*}_{xxxx}(-\omega_4;\omega_1,\omega_2,-\omega_3) \simeq \chi^{(3)}_{xxxx}(-\omega_3;\omega_1,\omega_2,-\omega_4)$.

The solutions of Equations 8a and b are obtained following the procedure discussed previously for parametric three-photon interactions [23].

$$E_0(\omega_4,z) = \exp\left(-\frac{\alpha_g z}{4}+\frac{i\Delta kz}{2}\right) \times\left\{E_0(\omega_3,0)\left[\cosh(\gamma z)+\left(\frac{\alpha_4-\alpha_3}{4\gamma}-\frac{i\Delta k}{2\gamma}\right)\sinh(\gamma z)\right]-E_0^*(\omega_4,0)\frac{igx}{2}\left(\frac{n_4\omega_3}{n_3\omega_4}\right)^{1/2}\sinh(\gamma z)\right\} \tag{9a}$$

$$E_0^*(\omega_4,z) = \exp\left(-\frac{\alpha_g z}{4}-\frac{i\Delta kz}{2}\right) \times\left\{E_0^*(\omega_4,0)\left[\cosh(\gamma z)-\left(\frac{\alpha_4-\alpha_3}{4\gamma}-\frac{i\Delta k}{2\gamma}\right)\sinh(\gamma z)\right]+E_0(\omega_3,0)\frac{ig^*\chi}{2\gamma}\left(\frac{n_3\omega_4}{n_4\omega_3}\right)^{1/2}\sinh(\gamma z)\right\} \tag{9b}$$

where

$$\chi = \chi^{(3)}_{xxxx}(-\omega_3;\omega_1,\omega_2,-\omega_4) \simeq \chi^{(3)*}_{xxxx}(-\omega_4;\omega_1,\omega_2,\omega_3) \tag{9c}$$

$$g = \frac{4\pi}{c}\left(\frac{\omega_3\omega_4}{n_3n_4}\right)^{1/2}E_{01}E_{02};\quad gg^* = \frac{1024\pi^4\omega_3\omega_4}{c^4n_1n_2n_3n_4}I_{01}I_{02} \tag{9d}$$

$$\gamma = 0.25\{\alpha_g^2+4[gg^*\chi^2-\alpha_3\alpha_4-\Delta k^2-i\Delta k(\alpha_4-\alpha_3)]\}^{1/2} \tag{9e}$$

$$\alpha_g = \alpha_3+\alpha_4 \tag{9f}$$

$$\Delta k = k_3+k_4-k_1-k_2 \tag{9g}$$

$$I_{0\nu} = \frac{n_\nu c}{8\pi}|E_{0\nu}|^2. \tag{9h}$$

In our experiments neither signal light at frequency ω_3 nor idler light at frequency ω_4 are incident on the sample. The parametric interaction starts from quantum fluctuations [23–25]. The spectral energy densities ϵ (energy per area and frequency interval, units e.g. J/cm^{2}s^{-1}) are given by:

$$\epsilon(\omega_3,z) = \epsilon_N(\omega_4)\exp\left(-\frac{\alpha_g z}{2}\right)\frac{|g\chi|^2\omega_3}{4|\gamma|^2\omega_4}|\sinh(\gamma z)|^2 \tag{10a}$$

$$\epsilon(\omega_4,z) = \epsilon_N(\omega_3)\exp\left(-\frac{\alpha_g z}{2}\right)\frac{|g\chi|^2\omega_4}{4|\gamma|^2\omega_3}|\sinh(\gamma z)|^2. \tag{10b}$$

The relation between the spectral energy densities $\epsilon(\omega)$ and the temporal intensities $I(t)$ and between the field strengths $E(\omega)$ and $E(t)$ are derived in the Appendix.

The solutions of the signal and idler light are quite similar. The linear absorption loss enters in the exponential damping factor and in the amplification factor γ. The factor γ contains the phase-mismatch Δk and the complex nonlinear susceptibility χ. If the gain factor $g\chi$ is large enough, the losses due to absorption and phase-mismatch can be compensated and amplification results. At high enough laser

intensities, for $|\gamma z| \gg 1$, the signal and idler light grow nearly exponentially. The nonlinear susceptibility χ is complex. The real part of $\chi^{(3)}$ is responsible for parametric interaction. When χ is purely imaginary no parametric gain is possible because of the negative sign of $gg^*\chi^2$ under the square root in Equation 9e. For negligible linear absorption and phase-mismatch Equations 10a and b simplify to:

$$\epsilon(\omega_3, z) = \epsilon_N(\omega_4)\frac{\omega_3}{\omega_4}|\sinh(|g|\chi z/2)|^2 \tag{11a}$$

$$\epsilon(\omega_4, z) = \epsilon_N(\omega_3)\frac{\omega_4}{\omega_3}|\sinh(|g|\chi z/2)|^2. \tag{11b}$$

These equations indicate exponential amplification for signal and idler light when $|g|\chi z \gg 1$.

To evaluate 10a, 10b or 11a and 11b, the spectral energy density of the quantum fluctuations ϵ_N has to be known. The energy density per unit frequency (units e.g. $J/(cm^3 s^{-1})$) has the form [26, 27]

$$u(\omega) = \frac{\hbar\omega^3 n^3}{2\pi^2 c^3}\Delta\Omega. \tag{12}$$

The spectral energy density of the quantum fluctuations is $\epsilon_N(\omega) \simeq u(\omega)c\Delta t_p/n(\omega)$; ($\Delta t_p$ is the duration of the pump pulse, $n(\omega)$ is the refractive index at frequency ω). Together with Equation 12 we obtain for ϵ_N (units e.g. $J/(cm^2 s^{-1})$):

$$\epsilon_N(\omega_i) \simeq \frac{\hbar\omega_i^3 n_i^3}{2\pi^2 c^2 n_p}\Delta t_p \Delta\Omega_i \tag{13}$$

where i stands for 3 or 4. The solid angle of the idler light can be expressed by the solid angle of the sign signal light [26, 27]: $\Delta\Omega_4 = (\omega_3^2/\omega_4^2)\Delta\Omega_3$ ($\Delta\Omega_3 \simeq 10^{-3}$ in our case).

The energy density of the quantum fluctuations per unit wave number is approximately $\epsilon_N(\tilde{\nu}_i) \simeq 10^{-14}$ J/cm ($\Delta t_p \simeq 6$ ps; $\tilde{\nu}_i \simeq 10^4$ cm^{-1}). The pump pulse energy density is about 0.6 J/cm^2 for $I_{0L} = 10^{11}$ W/cm^2 and $\Delta t_p = 6$ ps. An amplification of the quantum noise by a factor of $10^9 \simeq \exp(20)$ within a spectral range of 10^4 cm^{-1} depletes the pump laser by parametric light generation. Without absorption losses a gain factor of $|g|\chi z \simeq 20$ is sufficient for saturation of the parametric four-photon light production. At $I_{0L} = 10^{11}$ W/cm^2 and $z = 2$ cm, this gain value is reached for $\chi^{(3)} \simeq 2 \times 10^{-14}$ cm^3/erg. This value is typical for the nonresonant susceptibility of the substances investigated.

2.2.2. Saturation of parametric four-photon interaction $\omega_L + \omega_L \rightarrow \omega_3 + \omega_4$.

The (nearly) exponential amplification of signal and idler light at high pump intensities readily causes depletion of the laser light [28]. The laser fields E_{01} and E_{02} in Equations 8a and 8b are not constant during the interaction process.

To get approximate solutions we make the simplifying assumptions that $E(\omega_3)$, $E(\omega_4)$, α_3, α_4, Δk and $\chi^{(3)}$ are constant over the whole spectral range $\Delta\omega_3 = \Delta\omega_4 = \Delta\omega$. With the notation $E_{0i} = 1/(2\pi)\int_{-\infty}^{\infty} E_0(\omega_i)\,d\omega_i = 1/(2\pi)E_0(\omega_i)\Delta\omega$, ($i = 3, 4$), we obtain from Equations 7, 8a and b:

$$\frac{\partial E_{0L}}{\partial z} = -\frac{\alpha_L}{2}E_{0L} - \frac{i2\pi\omega_L}{n_L c}\chi_L^{(3)}E_{0L}^* E_{03}E_{04}\exp(-i\Delta kz) \tag{14a}$$

$$\frac{\partial E_{03}}{\partial z} = -\frac{\alpha_3}{2}E_{03} - \frac{i2\pi\omega_3}{n_3 c}\chi^{(3)}E_{04}^* E_{0L}^2\exp(i\Delta kz) \tag{14b}$$

$$\frac{\partial E_{04}^*}{\partial z} = -\frac{\alpha_4}{2}E_{04}^* + \frac{i2\pi\omega_4}{n_4 c}\chi^{(3)}E_{03}E_{0L}^{*2}\exp(-i\Delta kz) \tag{14c}$$

The abbreviations $\chi_L^{(3)} = \chi_{xxxx}^{(3)}(-\omega_L; -\omega_L, \omega_3, \omega_4)$ and $\chi^{(3)} = \chi_{xxxx}^{(3)}(-\omega_3; \omega_L, \omega_L, -\omega_4) \simeq \chi_{xxxx}^{(3)*}(-\omega_4; \omega_L, \omega_L, -\omega_3)$ have been used in Equations 14a, b and c.

The coupled differential equations may be further simplified by rewriting the complex quantities in

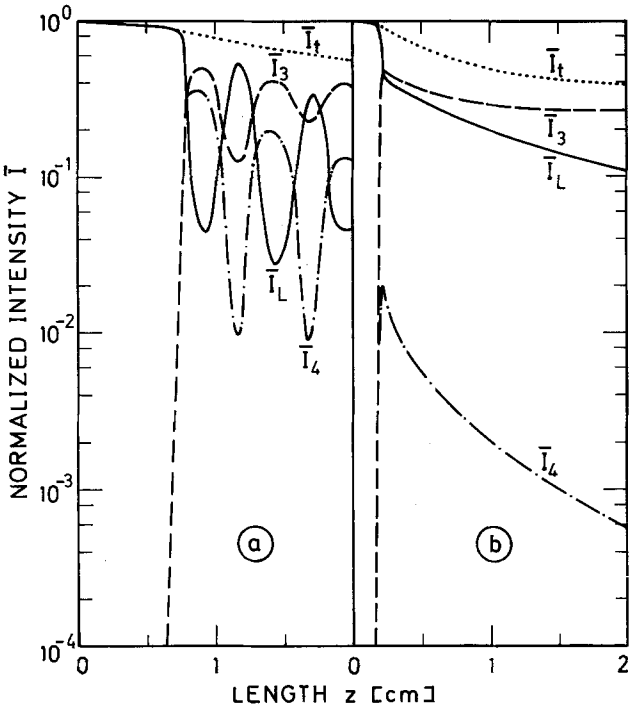

Figure 1 Calculation of the build-up of parametric light in the saturation range ($I_L = 2 \times 10^{11}$ W/cm^2). The curves represent the normalized pump pulse intensity $\bar{I}_L$ (full line), normalized signal intensity $\bar{I}_3$ (dashed line), normalized idler intensity $\bar{I}_4$ (dash-dot line), and normalized total intensity $\bar{I}_t$ (dotted line). The parameters used in the calculations are related to the interaction in water ($\alpha_L = 0.15\,\text{cm}^{-1}$) at two fixed frequencies with a bandwidth of 1000 cm^{-1}. (a) A situation of low phase-mismatch is considered. The parameters used are $\tilde{\nu}_3 = 10\,811\,\text{cm}^{-1}$, $\alpha_3 = 0.09\,\text{cm}^{-1}$, $\alpha_4 = 1.3\,\text{cm}^{-1}$, $\Delta k = 3.3\,\text{cm}^{-1}$, $\chi^{(3)\prime} = -8 \times 10^{-14}$ e.s.u., $\chi^{(3)\prime\prime} = -3 \times 10^{-15}$ e.s.u. (b) A situation of strong idler absoprtion and zero phase-mismatch is depicted. The parameters are $\tilde{\nu}_3 = 17\,160\,\text{cm}^{-1}$, $\alpha_3 = 0.001\,\text{cm}^{-1}$, $\alpha_4 = 400\,\text{cm}^{-1}$, $\Delta k = 0$, $\chi^{(3)\prime} = -9 \times 10^{-13}$ e.s.u., $\chi^{(3)\prime\prime} = -8 \times 10^{-13}$ e.s.u.

amplitudes and phases and by separating the real and imaginary parts. After some straightforward calculations, the following set of equations is obtained [16].

$$\frac{\partial \tilde{E}_L}{\partial z} = -\frac{\alpha_L}{2}\tilde{E}_L - \frac{2\pi\omega_L}{n_L c}\tilde{\chi}\tilde{E}_L\tilde{E}_3\tilde{E}_4 \sin(\theta + \phi_{SL}) \tag{15a}$$

$$\frac{\partial \tilde{E}_3}{\partial z} = -\frac{\alpha_3}{2}\tilde{E}_3 + \frac{2\pi\omega_3}{n_3 c}\tilde{\chi}\tilde{E}_L^2\tilde{E}_4 \sin(\theta + \phi_S) \tag{15b}$$

$$\frac{\partial \tilde{E}_4}{\partial z} = -\frac{\alpha_4}{2}\tilde{E}_4 + \frac{2\pi\omega_4}{n_4 c}\tilde{\chi}\tilde{E}_L^2\tilde{E}_3 \sin(\theta - \phi_S) \tag{15c}$$

$$\frac{\partial \theta}{\partial z} = -\frac{2\pi}{c}\left[\frac{2\omega_L}{n_L}\tilde{\chi}_L\tilde{E}_3\tilde{E}_4 \cos(\theta - \phi_{SL}) - \frac{\omega_3}{n_3}\tilde{\chi}\frac{\tilde{E}_L^2\tilde{E}_4}{\tilde{E}_4}\cos(\theta + \phi_S) - \frac{\omega_4}{n_4}\tilde{\chi}\frac{\tilde{E}_L^2\tilde{E}_3}{\tilde{E}_4}\cos(\theta - \phi_S)\right] + \Delta k. \tag{15d}$$

The relations $\tilde{E}_\nu = |E_{0\nu}|$, $E_{0\nu} = \tilde{E}_\nu \exp(i\phi_\nu)(\nu = L, 3, 4)$, $\tilde{\chi} = |\chi|$, $\chi = \tilde{\chi}\exp(i\phi_S) = 3\chi_{NR}^{(3)} + \chi_I^{(3)} + \chi_R^{(3)}$, $\tilde{\chi}_L = |\chi_L|$, $\chi_L = \tilde{\chi}_L \exp(i\phi_{SL}) = 6\chi_{NR}^{(3)} + 2\chi_I^{(3)*} + \chi_R^{(3)} + \chi_R^{(3)*}$ (see later), and $\theta = \Delta kz + 2\phi_L - \phi_3 - \phi_4$ are used. The initial phase was set to $\theta(0) = \pi/2$ [20]. The equations 15a–d were solved by numerical integration; normalized intensities $\bar{I}_\nu = I_\nu(z)/I_L(0)$ were evaluated.

In Fig. 1 numerical results of the spatial development for pump, signal and idler intensities are presented. The two sets of parameters listed in the figure captions of Figs 1a and b are relevant for four-

photon interaction in water (see below). Fig. 1a depicts the situation of small phase-mismatch and small idler absorption at $\tilde{\nu}_3 = 10\,811\,\mathrm{cm}^{-1}$ ($\tilde{\nu}_4 = 8100\,\mathrm{cm}^{-1}$). After a certain interaction length z the intensity of the signal and idler rises rapidly while the laser becomes strongly depleted. When the signal and idler light increase beyond the intensity of the depleted pump pulse and when the phase relationship between the waves allows it, the reverse process $\omega_3 + \omega_4 \rightarrow \omega_L + \omega_L$ sets in, i.e. signal and idler light are converted to pump light. An oscillating behaviour along the interaction path results [16]. In Fig. 1b the case of large idler absorption and perfect phase-matching with $\tilde{\nu}_3 = 17\,160\,\mathrm{cm}^{-1}$ and $\tilde{\nu}_4 = 1750\,\mathrm{cm}^{-1}$ is illustrated. Again, signal and idler light start rapidly until depletion of laser light sets in. The reduction of pump intensity prevents further generation of parametric light. The generated idler light suffers high absorption and its output is drastically reduced. The curves in Fig. 1 show that the total light output I_t is reduced more strongly than expected by the linear absorption of laser light. The continuous conversion of laser light into the idler region and the strong infrared absorption in this wavelength range are responsible for the reduced light output.

2.3. Four-photon frequency conversion $\omega_1 + \omega_2 + \omega_\gamma \rightarrow \omega$.

In the frequency conversion process two strong pump waves at frequencies ω_1 and ω_2 (width $\Delta\omega_1$ and $\Delta\omega_2$; special case $\omega_1 = \omega_2 = \omega_L$) and a weak wave at frequency ω_γ, (width $\Delta\omega_\gamma$, idler pulse) interact in the sample and produce light at a new signal frequency $\omega_1 + \omega_2 + \omega_\gamma$ ($\omega_\alpha = \omega_1$, $\omega_\beta = \omega_2$). The signal and idler light produced in the four-photon process of the previous Section 2.2. may act as input wave at ω_γ for frequency conversion. In this way light at frequencies $\omega > 2\omega_L$ is generated.

We consider the case where the frequency conversion process does not deplete the pump pulses and where no linear absorption of the pump waves occurs ($\alpha_1 = \alpha_2 = 0$). Equations 7 reduce to two coupled differential equations:

$$\frac{\partial E_0(\omega)}{\partial z} = -\frac{\alpha}{2}E_0(\omega) - \frac{i2\pi\omega}{nc}\chi^{(3)}_{xxxx}(-\omega;\omega_1,\omega_2,\omega_\gamma)E_0(\omega_\gamma)E_{01}E_{02}\exp(i\Delta kz) \tag{16a}$$

$$\frac{\partial E_0(\omega_\gamma)}{\partial z} = -\frac{\alpha_\gamma}{2}E_0(\omega_\gamma) - \frac{i2\pi\omega_\gamma}{n_\gamma c}\chi^{(3)}_{xxxx}(-\omega_\gamma;-\omega_1,-\omega_2,\omega)E_0(\omega_\gamma)E^*_{01}E^*_{02}\exp(-i\Delta kz) \tag{16b}$$

We shall show below that $\chi^{(3)}_{xxxx}(-\omega;\omega_1,\omega_2,\omega_\gamma) \simeq \chi^{(3)}_{xxxx}(-\omega_\gamma,-\omega_1,-\omega_2,\omega)$. Solutions of Equations 16a and b are found by following the procedure for three-photon frequency conversion [23].

$$E_0(\omega,z) = \exp\left(-\frac{\alpha_g z}{4} + \frac{i\Delta kz}{2}\right)$$
$$\times\left\{E_0(\omega,0)\left[\cosh(\gamma z) + \left(\frac{\alpha_\gamma-\alpha}{4\gamma}+\frac{i\Delta k}{2\gamma}\right)\sinh(\gamma z)\right] - E_{0\gamma}(\omega,0)\frac{ig\chi}{2\gamma}\left(\frac{n_\gamma\omega}{n\omega_\gamma}\right)^{1/2}\sinh(\gamma z)\right\} \tag{17a}$$

$$E_0(\omega_\gamma,z) = \exp\left(-\frac{\alpha_g z}{4} - \frac{i\Delta kz}{2}\right)$$
$$\times\left\{E_{0\gamma}(\omega,0)\left[\cosh(\gamma z) + \left(\frac{\alpha-\alpha_\gamma}{4\gamma}+\frac{i\Delta k}{2\gamma}\right)\sinh(\gamma z)\right] - E_0(\omega,0)\frac{ig^*\chi}{2\gamma}\left(\frac{n\omega_\gamma}{n_\gamma\omega}\right)^{1/2}\sinh(\gamma z)\right\} \tag{17b}$$

where

$$g = (4\pi/c)[\omega\omega_\gamma/(n_\gamma n)]^{1/2}E_{01}E_{02} \tag{17c}$$

$$\chi = \chi^{(3)}_{xxxx}(-\omega;\omega_1,\omega_2,\omega_\gamma) \simeq \chi^{(3)}_{xxxx}(-\omega_\gamma;-\omega_1,-\omega_2,\omega) \tag{17d}$$

$$\gamma = 0.25\{\alpha_g^2 - 4[gg^*\chi^2 + \alpha\alpha_\gamma + \Delta k^2 + i\Delta k(\alpha-\alpha_\gamma)]\}^{1/2} \tag{17e}$$

$$\alpha_g = \alpha + \alpha_\gamma; \quad \Delta k = k - k_1 - k_2 - k_\gamma$$

The initial conditions are $E_0(\omega,0) = 0$ and $E_0(\omega_\gamma,0) \neq 0$. The energy density generated at frequency

$\omega = \omega_1 + \omega_2 + \omega_\gamma$ is then given by:

$$\epsilon(\omega, z) = \frac{cn}{4\pi^2}|E_0(\omega, z)|^2$$

$$= \epsilon(\omega_\gamma, 0)\exp\left(-\frac{\alpha_g z}{2}\right)\frac{gg^*\chi\chi^*\omega}{4\gamma\gamma^*\omega_\gamma}|\sinh(\gamma z)|^2 \tag{18}$$

where $\epsilon(\omega_\gamma,0)$ is the initial spectral energy density at frequency ω_γ. The linear absorption is described by the exponential absorption loss factor. Absorption and phase-mismatch Δk reduce the conversion efficiency. The situation is greatly simplified when the frequencies ω, ω_γ, ω_1 and ω_2 are far from material resonances. In this case, linear absorption ($\alpha = \alpha_\gamma = 0$) and phase mismatch Δk (small colour dispersion) may be neglected and χ is a real quantity (γ imaginary). From Equation 18 we obtain for $\epsilon(\omega, 0) = 0$:

$$\epsilon(\omega, z) = \epsilon(\omega_\gamma 0)(\omega/\omega_\gamma)\sin^2(|g|\chi z/2) \tag{19a}$$

$$\epsilon(\omega_\gamma, z) = \epsilon(\omega_\gamma 0)\cos^2(|g|\chi z/2). \tag{19b}$$

Equations 19 describe the parametric frequency conversion process where new light at frequency ω is generated until the input pulse at ω_γ is depleted ($|g|\chi z = \pi$). The reverse process $\omega \rightarrow \omega_1 + \omega_2 + \omega_\gamma$ takes place for a longer interaction length ($\pi < |g|\chi z < 2\pi$). The pump intensity remains constant as long as the total input intensity, $\int \epsilon(\omega_\gamma, 0)\, d\omega_\gamma$, is small compared to the laser pump.

Recently four-photon frequency up-conversion $2\omega_L + \omega_\gamma \rightarrow \omega$ of weak infrared light at ω_γ was investigated in metal vapours [29]. Two-photon resonances at $2\omega_L$ were employed to enhance the conversion efficiency.

2.4. Three-frequency mixing $\omega_L + \omega_L \pm \omega_R \rightarrow \omega$.

We consider the case where two intense light pulses with central frequencies ω_L and ω_R and spectral widths $\Delta\omega_L$ and $\Delta\omega_R$ are incident on the sample and new light is generated at $\omega = 2\omega_L \pm \omega_R$. ($\omega_\alpha = \omega_\beta = \omega_L$, $\omega_\gamma = \pm\omega_R$). The light conversion efficiency should be small, i.e. depletion of the waves at frequencies ω_L (laser pulse) and ω_R (e.g. Raman Stokes pulse) does not occur ($\alpha_L = \alpha_R = 0$ is assumed).

2.4.1. Sum frequency generation $\omega_L + \omega_L + \omega_R \rightarrow \omega$.

We repeat, in contrast to the frequency conversion discussed in Section 2.3, the incident wave at ω_R is intense and is not depleted in the mixing process. With E_{0L} and E_{0R} both constant we obtain from Equation 7 for the peak electric field E_0 of the generated light:

$$\frac{\partial E_0}{\partial z} = -\frac{\alpha}{2}E_0 - \frac{i2\pi\omega}{nc}\chi^{(3)}_{xxxx}(-\omega; \omega_L, \omega_L, \omega_R)E_{0L}^2 E_{0R}\exp(i\Delta kz) \tag{20}$$

The solution of Equation 20 is found by integration.

$$E_0\left(t - \frac{zn}{c}, z\right) = \frac{i2\pi\omega}{nc}\chi^{(3)}_{xxxx}(-\omega; \omega_L, \omega_L, \omega_R)E_{0L}^2 E_{0R} \times \left[\exp\left(-\frac{\alpha z}{2}\right) - \exp(i\Delta kz)\right] \Big/ \left(\frac{\alpha}{2} + i\Delta k\right). \tag{21}$$

For a negligibly small value of the absorption coefficient α at $\omega = 2\omega_L + \omega_R$, Equation 21 simplifies and we obtain for the intensity of the generated light

$$I\left(t - \frac{zn}{c}, z\right) = \frac{cn}{8\pi}\left|E_0\left(t - \frac{zn}{c}; z\right)\right|^2$$

$$= \frac{256\pi^4\omega^2}{c^4 n n_L^2 n_R}|\chi^{(3)}_{xxxx}(-\omega; \omega_L, \omega_L, \omega_R)|^2 I_{0L}^2 I_{0R}\frac{\sin^2(\Delta kz/2)}{(\Delta k/2)^2}. \tag{22}$$

The light generation is determined by the square of the linear susceptibility $\chi^{(3)}$. The real as well as the

imaginary part of $\chi^{(3)}$ contributes to frequency mixing. The light generation at ω is most effective for $\Delta k = k - 2k_L - k_R = 0$ where $\sin^2(\Delta kz/2)/(\Delta k/2)^2 = z^2$. In general, we have $\Delta k \neq 0$. In this case we have a periodic spatial exchange of photons between the low frequency input at ω_R and the high frequency output at ω; i.e. both processes $\omega_L + \omega_L + \omega_R \rightarrow \omega$ and $\omega \rightarrow \omega_L + \omega_L + \omega_R$ take place. The generated light reaches its maxima at $z = (2m + 1)\pi/\Delta k$ (where m is an integer). The length $l_c = \pi/|\Delta k| = \pi c/(|n\omega - 2n_L\omega_L - n_R\omega_R|)$ is called the coherence length. In isotropic media the coherence length for three-frequency mixing is typically a few 10^{-4} cm i.e. several laser wavelengths. This short interaction does not allow large conversion efficiencies. The assumption of undepleted waves is certainly correct.

Phase-matched three-frequency mixing $2\omega_L + \omega_R$ with tunable lasers in metal vapours and gases was studied for the generation of light in the vacuum ultra-violet [30–32]. Two-photon resonances at $2\omega_L$ were utilized by tuning one laser frequency to a two-photon allowed electronic transition at $2\omega_L$. Electronic single frequency resonances (e.g. autoionization states) in the neighbourhood of $\omega = 2\omega_L + \omega_R$ enhance the ultraviolet generation even further.

2.4.2. Difference frequency generation $\omega_L + \omega_L - \omega_R \rightarrow \omega$.

In the difference frequency mixing process an intense light pulse at frequency ω_R (band width $\Delta\omega_R$) is incident on the medium while in the parametric four-photon interaction of Section 2.2. quantum noise or weak input signals are amplified.

The equations for the difference frequency generation are the same as for the sum frequency mixing if the following changes are made: $\chi^{(3)}(-\omega; \omega_L, \omega_L, \omega_R) \rightarrow \chi^{(3)}(-\omega; \omega_L, \omega_L, -\omega_R)$, $E_{0R} \rightarrow E_{0R}^*$ and $\Delta k \rightarrow k + k_R - 2k_L$.

Recently, various difference frequency mixing experiments with tunable lasers were carried out. Mixing processes $\omega = 2\omega_L - \omega_R$ with vibrational resonances at $\omega_L - \omega_R$ were investigated and the dispersion of the nonlinear susceptibility $\chi^{(3)}$ around Raman-type resonances was studied [33–35]. The difference frequency mixing spectroscopy $\omega = 2\omega_L - \omega_R$ with fixed frequency ω_L and tunable frequency $\omega_R < \omega_L$ became a sensitive Raman technique and was called coherent anti-Stokes Raman spectroscopy (CARS) [36–38].

2.5. Third harmonic generation $\omega_L + \omega_L + \omega_L \rightarrow \omega$.

A light pulse with central frequency ω_L and spectral width $\Delta\omega_L$(FWHM) enters the sample and light at $\omega = 3\omega_L$ is generated ($\omega_\alpha = \omega_\beta = .\omega_\gamma = \omega_L$). The pump wave should not be depleted and $\alpha_L = 0$ is assumed.

The differential equation for third harmonic generation and its solution is identical to the case of three-frequency mixing when ω_R is replaced by ω_L. The remarks following Equation 20 apply to third harmonic generation as well.

Recently, phase-matched third harmonic generation in metal vapours has been of considerable interest [39–41]. Intensity conversions of up to several per cent could be obtained. Electronic two-photon resonances at $2\omega_L$ were employed for VUV-generation.

3. Resonant structure of $\chi^{(3)}$.

3.1. General

The nonlinear susceptibility $\chi^{(3)}_{xxxx}(-\omega, \omega_\alpha, \omega_\beta, \omega_\gamma)$ is discussed in this section. The absolute value of the coupling parameter $\chi^{(3)}$ and the frequency dependence of the real and imaginary part of $\chi^{(3)}$ determine the energy conversion and the spectral distribution of the parametrically generated light.

$\chi^{(3)}$ is obtained by a quantum mechanical calculation of the induced polarization. We consider only electric dipole interactions. An expression for the induced polarization is obtained by time-dependent perturbation theory. In particular, the nonlinear polarization $P^{(3)}_{NL} = \chi^{(3)}_0 EEE$ is obtained by third order perturbation theory. The component of the nonlinear susceptibility $\chi^{(3)}$ (equal to $0.25\chi^{(3)}_0$ [18, 19]), which enters our Equation 7 has the general form [18, 19]:

$$\chi^{(3)}_{xxxx}(-\omega;\omega_\alpha,\omega_\beta,\omega_\gamma) = \frac{NL\,e^4}{8\hbar^3}\sum_P\sum_{a,b,c}\left[\frac{\langle g|x|a\rangle\langle a|x|b\rangle\langle b|x|c\rangle\langle c|x|g\rangle}{(\omega_a-\omega)(\omega_b-\omega_k-\omega_l)(\omega_c-\omega_l)}\right.$$
$$+\frac{\langle g|x|a\rangle\langle a|x|b\rangle\langle b|x|c\rangle\langle c|x|g\rangle}{(\omega_a^*+\omega_j)(\omega_b-\omega_k-\omega_l)(\omega_c-\omega_l)}$$
$$+\frac{\langle g|x|c\rangle\langle c|x|b\rangle\langle b|x|a\rangle\langle a|x|g\rangle}{(\omega_a^*+\omega)(\omega_b^*+\omega_k+\omega_l)(\omega_c^*+\omega_l)}$$
$$\left.+\frac{\langle g|x|c\rangle\langle c|x|b\rangle\langle b|x|a\rangle\langle a|x|g\rangle}{(\omega_a-\omega_j)(\omega_b^*+\omega_k+\omega_l)(\omega_c^*+\omega_l)}\right]. \tag{23}$$

N is the number of molecules per unit volume [$1/cm^3$], $L \simeq (n^2+2)/3 \times (n_\alpha^2+2)/3 \times (n_\beta^2+2)/3 \times (n_\gamma^2+2)/3$ is the local field correction factor. The first sum runs over all permutations, ω_j, ω_k and ω_l of the frequencies ω_α, ω_β and ω_γ. The second triple sum runs over all excited states of the system. ω_a, ω_b, and ω_c are excited state frequencies. These frequencies are complex quantities $\omega_\nu = \Omega_\nu - i\Gamma_\nu$; $\nu = a, b,$ or c. The real part Ω_ν is equal to a transition frequency from the ground state, the imaginary part Γ_ν describes the relaxation processes [18, 19]. The terms in the sum contain a product of four matrix elements in the numerator and a product of three frequency terms in the denominator. $\chi^{(3)}_{xxxx}(-\omega;\omega_\alpha,\omega_\beta,\omega_\gamma)$ is approximately independent of frequency and is nearly real except when the frequencies ω, ω_α, ω_β, ω_γ or the sums $2\omega_\alpha$, $2\omega_\beta$, $2\omega_\gamma$, $\omega_\alpha+\omega_\gamma$ or $\omega_\beta+\omega_\gamma$ are near an excited state frequency. In the latter case large resonant terms appear. $\chi^{(3)}$ may be separated in a non-resonant part $D\chi^{(3)}_{NR}$, a part comprising single frequency resonances $\chi^{(3)}_I$ and a part combining resonances due to sum (or difference) frequencies $\chi^{(3)}_R$.

$$\chi^{(3)} = D\chi^{(3)}_{NR} + \chi^{(3)}_I + \chi^{(3)}_R. \tag{24}$$

We have $D = 6$ when the three frequencies ω_α, ω_β and ω_γ are different, $D = 3$ when two frequencies are equal and $D = 1$ when all three frequencies are equal [18, 19].

In the following subsections we discuss the frequency dependence of $\chi^{(3)}$ relevant for the parametric processes described in Section 2. We concentrate on resonances which occur in the substances studied in our experiments.

3.2. Parametric four-photon interaction $\omega_L + \omega_L \rightarrow \omega_3 + \omega_4$.

In Section 2.2. we introduced the susceptibilities $\chi^{(3)}_{xxxx}(-\omega_3;\omega_1,\omega_2,-\omega_4)$, $\chi^{(3)}_{xxxx}(-\omega_4;\omega_1,\omega_2,-\omega_3)$, $\chi^{(3)}_{xxxx}(-\omega_1;-\omega_2,\omega_3,\omega_4)$, and $\chi^{(3)}_{xxxx}(-\omega_2;-\omega_1,\omega_3,\omega_4)$. The frequencies ω_1, ω_2, $2\omega_1$, $2\omega_2$, and $\omega_1+\omega_2$ of our experiments are far away from excited state frequencies and do not contribute to the resonant structure of $\chi^{(3)}$.

Single frequency resonance terms occur when the idler frequency ω_4 lies in the range of infrared absorption bands. The contributions of single frequency resonances to $\chi^{(3)}(-\omega_3;\omega_1,\omega_2;-\omega_4)$ are:

$$\chi^{(3)}_{I,xxxx}(-\omega_3;\omega_1,\omega_2,-\omega_4) = \frac{NL\,e^4}{8\hbar^3}\sum_{\bar c}\frac{1}{\omega_{\bar c}^*-\omega_4}\sum_{a,b}\langle g|x|\bar c\rangle\langle\bar c|x|b\rangle\langle b|x|a\rangle\langle a|x|g\rangle$$
$$\times\left[\frac{1}{(\omega_a^*+\omega_3)(\omega_b^*+\omega_1-\omega_4)}+\frac{1}{(\omega_a^*+\omega_3)(\omega_b^*+\omega_2-\omega_4)}+\frac{1}{(\omega_a-\omega_1)(\omega_b^*+\omega_2-\omega_4)}\right.$$
$$\left.+\frac{1}{(\omega_a^*-\omega_2)(\omega_b^*+\omega_1-\omega_4)}+\frac{1}{(\omega_a-\omega_1)(\omega_b-\omega_1-\omega_2)}+\frac{1}{(\omega_a-\omega_2)(\omega_b-\omega_1-\omega_2)}\right] \tag{25a}$$
$$\simeq \frac{NL\,e^4}{8\hbar^3}K\sum_{\bar c}\langle g|x|\bar c\rangle\langle\bar c|x^3|g\rangle\left[\frac{\Omega_{\bar c}-\omega_4}{(\Omega_{\bar c}-\omega_4)^2+\Gamma_{\bar c}^2}-\frac{i\Gamma_{\bar c}}{(\Omega_{\bar c}-\omega_4)^2+\Gamma_{\bar c}^2}\right] \tag{25b}$$

$$= 2(\chi_{\mathrm{I}}^{(3)'} + i\chi_{\mathrm{I}}^{(3)''}) \tag{25c}$$

In Equation 25b the relations $\sum_a |a\rangle\langle a| = 1$ and $\sum_b |b\rangle\langle b| = 1$ were used. The frequencies ω_a and ω_b in the denominators were replaced by average frequency values. The six denominator terms are abbreviated by K which is approximately real and greater than zero since the average frequency values lie in the electronic absorption range. A slight frequency dependence of K is neglected. The matrix elements are approximately real.

It can be shown from Equation 23 that $\chi^{(3)}_{\mathrm{I},xxxx}(-\omega_3;\omega_1,\omega_2,-\omega_4)$ is approximately equal to $\chi^{(3)}_{\mathrm{I},xxxx}(-\omega_4;\omega_1,\omega_2,-\omega_3)$; $\chi^{(3)*}_{\mathrm{I},xxxx}(-\omega_1;-\omega_2,\omega_3,\omega_4)$ and $\chi^{(3)*}_{\mathrm{I},xxxx}(-\omega_2,-\omega_1,\omega_3,\omega_4)$ by neglecting the imaginary parts in the non-resonant frequency denominators. For the degenerate case $\omega_1 = \omega_2 = \omega_{\mathrm{L}}$ we find

$$\chi^{(3)}_{\mathrm{I},xxxx}(-\omega_3,\omega_{\mathrm{L}},\omega_{\mathrm{L}},-\omega_4) = \chi_{\mathrm{I}}^{(3)'} + \chi_{\mathrm{I}}^{(3)''} \simeq \chi^{(3)*}_{\mathrm{I},xxxx}(-\omega_4;\omega_{\mathrm{L}},\omega_{\mathrm{L}},-\omega_3)$$
$$\simeq \tfrac{1}{2}\chi^{(3)*}_{\mathrm{I},xxxx}(-\omega_{\mathrm{L}};-\omega_{\mathrm{L}},\omega_3,\omega_4).$$

The frequency dependence of the imaginary part $\chi_{\mathrm{I}}^{(3)''}$ may be related to the dispersion of the linear absorption coefficient. The maximum linear absorption coefficient at frequency $\Omega_{\bar{c}}$ is given by $\alpha(\Omega_{\bar{c}}) = \tilde{K}\langle g|x|\bar{c}\rangle\langle\bar{c}|x|g\rangle$ [42]. In Equation 25 $\chi_{\mathrm{I}}^{(3)}$ depends on $\langle g|x|\bar{c}\rangle\langle\bar{c}|x^3|g\rangle$. The following calculations show that $\langle\bar{c}|x^3|g\rangle$ is nearly proportional to $\langle\bar{c}|x|g\rangle$ i.e., $\langle g|x|\bar{c}\rangle\langle\bar{c}|x^3|g\rangle$ is proportional to $\alpha(\Omega_{\bar{c}})$: It is $\langle\bar{c}|x^3|g\rangle = \sum_j \langle\bar{c}|x|a_j\rangle\langle a_j|x^2|g\rangle \simeq \sum_l \langle\bar{c}|x|a_l\rangle\langle a_l|x^2|g\rangle = \langle\bar{c}|x|\bar{a}\rangle \times \sum_l \langle a_l|x^2|g\rangle = \langle\bar{c}|x|\bar{a}\rangle C_1 \simeq \langle\bar{c}|x|g\rangle C_2 \ldots C_1$ and C_2 are constants. The first sum runs over all states $|a_j\rangle$ with the same parity as $|g\rangle$ (other matrix elements are zero). In the second sum, only the states $|a_l\rangle$ are retained that form large matrix elements. These states $|a_l\rangle$ have a shape similar to $|g\rangle$. This fact implies that the average state $|\bar{a}\rangle$ is similar to $|g\rangle$ and that $\langle\bar{c}|x|\bar{a}\rangle \simeq$ const $\langle\bar{c}|x|g\rangle$. Now Equation 25 may be rewritten as

$$\chi^{(3)}_{\mathrm{I},xxxx}(-\omega_3;\omega_1,\omega_2,-\omega_4) \simeq C\sum_{\bar{c}} \alpha(\Omega_{\bar{c}})\Gamma_{\bar{c}}\frac{(\Omega_{\bar{c}}-\omega_4) - i\Gamma_{\bar{c}}}{(\Omega_{\bar{c}}-\omega_4)^2 + \Gamma_{\bar{c}}^2}. \tag{26}$$

$C > 0$ is constant. The slight frequency dependence of C is neglected. Equation 26 shows that $\chi^{(3)''}_{\mathrm{I},xxxx}(-\omega_3;\omega_1,\omega_2,-\omega_4)$ has the same frequency dependence as $-\alpha(\omega_4)$ since $\alpha(\omega_4) = \alpha(\Omega_{\bar{c}})\Gamma_{\bar{c}}^2/[(\Omega_{\bar{c}}-\omega_4)^2 + \Gamma_{\bar{c}}^2]$. The frequency dependence of the real part $\chi_{\mathrm{I}}^{(3)}$ is connected to the frequency dependence of the imaginary part $\chi_{\mathrm{I}}^{(3)''}$ by Equation 26. The absolute scale of $\chi^{(3)}_{\mathrm{I},xxxx}(-\omega_3;\omega_1,\omega_2,-\omega_4)$ must be determined experimentally by measuring the spectral signal intensity at a fixed set of frequencies $\omega_3,\omega_1,\omega_2,\omega_4$ and by calculating $\chi^{(3)}$ from Equation 10a.

Difference frequency resonances occur when $\omega_1 - \omega_4$ or $\omega_2 - \omega_4$ are near an excited state frequency of the system. The contributions of difference frequency resonances to $\chi^{(3)}$ are given by:

$$\chi^{(3)}_{\mathrm{R},xxxx}(-\omega_3;\omega_1,\omega_2,-\omega_4) = \frac{NL\mathrm{e}^4}{8\hbar^3}\sum_{\bar{b}}\frac{1}{\omega_{\bar{b}}-\omega_1+\omega_4}\sum_{a,c}\langle g|x|a\rangle\langle a|x|\bar{b}\rangle\langle\bar{b}|x|c\rangle\langle c|x|g\rangle$$
$$\times\left[\frac{1}{(\omega_a-\omega_3)(\omega_c+\omega_4)}+\frac{1}{(\omega_a-\omega_3)(\omega_c-\omega_1)}+\frac{1}{(\omega_a^*+\omega_2)(\omega_c+\omega_4)}+\frac{1}{(\omega_a^*+\omega_2)(\omega_c-\omega_1)}\right]$$
$$+\frac{1}{\omega_{\bar{b}}-\omega_2+\omega_4}\sum_{a,c}\langle g|x|a\rangle\langle a|x|\bar{b}\rangle\langle\bar{b}|x|c\rangle\langle c|x|g\rangle\times\left[\frac{1}{(\omega_a-\omega_3)(\omega_c+\omega_4)}+\frac{1}{(\omega_a-\omega_3)(\omega_c-\omega_2)}\right.$$
$$\left.+\frac{1}{(\omega_a^*+\omega_1)(\omega_c+\omega_4)}+\frac{1}{(\omega_a^*+\omega_1)(\omega_c-\omega_2)}\right]\Bigg)$$
$$\simeq \frac{NL\mathrm{e}^4}{8\hbar^3}\sum_{\bar{b}}\langle g|x^2|\bar{b}\rangle\langle\bar{b}|x^2|g\rangle\left[K_1\frac{\Omega_{\bar{b}}-\omega_1+\omega_4+i\Gamma_{\bar{b}}}{(\Omega_{\bar{b}}-\omega_1+\omega_4)^2+\Gamma_{\bar{b}}^2}+K_2\frac{\Omega_{\bar{b}}-\omega_2+\omega_4+i\Gamma_{\bar{b}}}{(\Omega_{\bar{b}}-\omega_2+\omega_4)^2+\Gamma_{\bar{b}}^2}\right]$$
$$= \chi'_{\mathrm{R}}(\omega_1)+\chi'_{\mathrm{R}}(\omega_2)+i[\chi''_{\mathrm{R}}(\omega_1)+\chi''_{\mathrm{R}}(\omega_2)]. \tag{27}$$

From Equation 23 we find $\chi^{(3)}_{R,xxxx}(-\omega_4;\omega_1,\omega_2,-\omega_3) \simeq \chi^{(3)*}_{R,xxxx}(-\omega_3;\omega_1,\omega_2,-\omega_4)$. $\chi^{(3)}_{R,xxxx}(-\omega_1;\omega_2,\omega_3,\omega_4) = \chi^{(3)*}_{R,xxxx}(-\omega_2;-\omega_1,\omega_3,\omega_4) = \chi'_R(\omega_1) + \chi'_R(\omega_2) \mp i[\chi''_R(\omega_1) + \chi''_R(\omega_2)]$ (negative for $\omega_1 > \omega_2 > \omega_4$ and positive for $\omega_1 > \omega_2 < \omega_4$). For $\omega_1 = \omega_2 = \omega_L$ the susceptibilities reduce to $\chi^{(3)}_R(-\omega_3;\omega_L,\omega_L,-\omega_4) = \chi^{(3)*}_R(-\omega_4;\omega_L,\omega_L,-\omega_3) \simeq \chi'_R(\omega_L) + i\chi''_R(\omega_L)$ and $\chi^{(3)}_R(-\omega_L;-\omega_L,\omega_3,\omega_4) = 2\chi^{(3)'}_R(\omega_L)$.

The imaginary part $\chi^{(3)''}_R(\omega_L)$ of the difference frequency resonance is equal to the Raman susceptibility [17]. $\chi^{(3)''}_R$ may be derived by spontaneous or stimulated Raman scattering. The real part $\chi^{(3)'}_R$ may be determined from the fixed relation between the real and the imaginary part of $\chi^{(3)}_R$ (see Equation 27). A small calculation leads to the following expression:

$$\chi^{(3)}_{R,xxxx}(-\omega_3;\omega_1,\omega_2,-\omega_4) \simeq$$

$$\sum_{\bar{b}} \chi''_R(\Omega_{\bar{b}})\Gamma_{\bar{b}} \times \left[\frac{(\Omega_{\bar{b}} - \omega_1 + \omega_4) + i\Gamma_{\bar{b}}}{(\Omega_{\bar{b}} - \omega_1 + \omega_4)^2 + \Gamma^2_{\bar{b}}} + \frac{(\Omega_{\bar{b}} - \omega_2 + \omega_4) + i\Gamma_{\bar{b}}}{(\Omega_{\bar{b}} - \omega_2 + \omega_4)^2 + \Gamma^2_{\bar{b}}}\right]. \tag{28}$$

$\chi''_R(\Omega_{\bar{b}})$ is the maximum value of the Raman susceptibility at vibrational frequency $\Omega_{\bar{b}}$. $\Gamma_{\bar{b}}$ is the half width of the Raman line. In Equation 28 we used the approximation $K_1 = K_2$.

Finally, the non-resonant part $\chi^{(3)}_{NR}$ originates from electronic transition frequencies in the ultraviolet. The dispersion of $\chi^{(3)}_{NR}(-\omega_3;\omega_L,\omega_L,-\omega_4)$ is governed by a term proportional to $1/[(\omega_{uv} - \omega_L) \times (\omega_{uv} - \omega_4)(\omega_{uv} - \omega_3)]$. We neglect the frequency dependence of $\chi^{(3)}_{NR}$, since the ultraviolet frequency ω_{uv} is considerably larger than the other frequencies $\omega_L, \omega_3, \omega_4$. The magnitude of $\chi^{(3)}_{NR}$ has been investigated by a variety of techniques: third harmonic generation [18, 19], intensity dependent rotation of elliptically polarized monochromatic light [18, 19, 43], self-focusing [44], interference patterns of beam profiles [45, 46], and coherent anti-Stokes Raman scattering [33–35].

The complete $\chi^{(3)}$ involved in the parametric four-photon interaction processes of Section 2.2 has the form:

$$\chi^{(3)}(-\omega_3;\omega_1,\omega_2,-\omega_4) \simeq \chi^{(3)*}(-\omega_4,\omega_1,\omega_2,-\omega_3)$$
$$= 6\chi^{(3)}_{NR} + 2(\chi^{(3)'}_I + i\chi^{(3)''}_I) + \chi^{(3)'}_R(\omega_1) + \chi^{(3)'}_R(\omega_2) + i[\chi^{(3)''}_R(\omega_1) + \chi^{(3)''}_R(\omega_2)];$$
$$\chi^{(3)}(-\omega_3;\omega_L,\omega_L,-\omega_4) = \chi^{(3)*}(-\omega_4,\omega_L,\omega_L,-\omega_3)$$
$$= 3\chi^{(3)}_{NR} + \chi^{(3)'}_I + i\chi^{(3)''}_I + \chi^{(3)'}_R(\omega_L) + i\chi^{(3)'}_R(\omega_L)$$

and

$$\chi^{(3)}(-\omega_L;-\omega_L,\omega_3,\omega_4) = 6\chi^{(3)}_{NR} + 2[\chi^{(3)'}_I + i\chi^{(3)''}_I + \chi^{(3)'}_R(\omega_L)].$$

In Figs 2a and b the real and imaginary parts of $\chi^{(3)}$ are shown schematically for the process $\omega_L + \omega_L \rightarrow \omega_3 + \omega_4$. The nonresonant part of $\chi^{(3)}$ is practically real and frequency independent. The real parts of the resonant terms are zero at the maxima of the imaginary parts. We recall that there is no parametric amplification of the four-photon process of Section 2.2, when the real part of $\chi^{(3)}$ is zero. The imaginary part of the resonant terms decreases proportional to $1/\omega_\nu^2$ while the real part of the resonant terms decreases proportional to $1/\omega_\nu$ (where $\omega_\nu = \Omega_\nu - \omega_4$, $\Omega_\nu - \omega_1 + \omega_4$, or $\Omega_\nu - \omega_2 + \omega_4$). As a result, the parametric amplification process (due to the real parts of $\chi^{(3)}$ persists far from the resonance frequencies.

3.3. Four-photon frequency conversion $\omega_1 + \omega_2 + \omega_\gamma \rightarrow \omega$

In the case of frequency conversion we consider the process $\omega_L + \omega_L + \omega_\gamma \rightarrow \omega$. The susceptibilities $\chi^{(3)}(-\omega;\omega_L,\omega_L,\omega_\gamma)$ and $\chi^{(3)}(-\omega_\gamma;\omega_L,\omega_L,\omega)$ are involved in the interaction (see Equations 16a and b). The frequencies $\omega_L, 2\omega_L, \omega_L + \omega_\gamma = \omega - \omega_L$, and ω are generally far away from the transition frequencies of the system. No sum or difference resonances occur and $\chi^{(3)}$ reduces to $3\chi^{(3)}_{NR} + \chi^{(3)}_I$.

Single frequency resonances have to be considered when ω_γ is near an infrared absorption band. The contribution of the single frequency resonances to $\chi^{(3)}$ is written in the form:

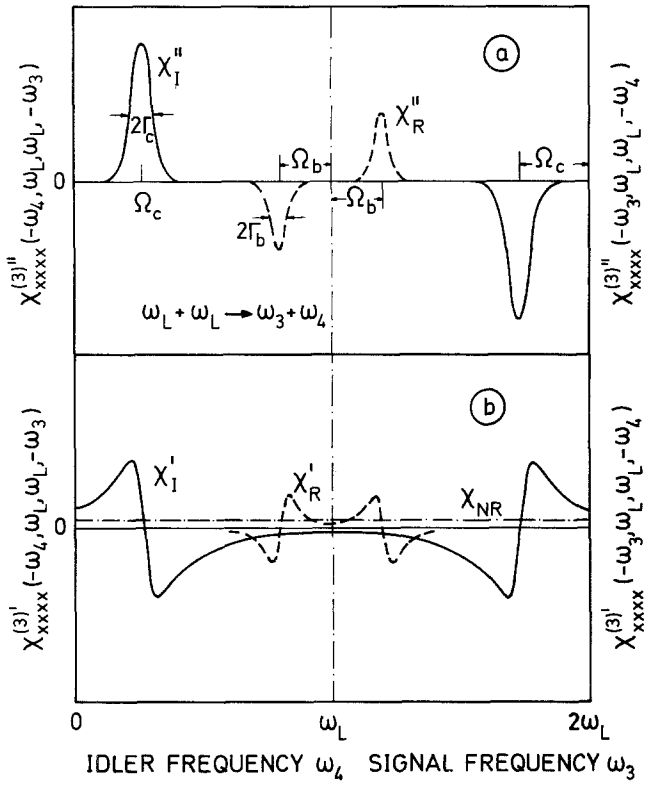

Figure 2 Diagram of the frequency dependence of the nonlinear susceptibility $\chi^{(3)}_{xxxx}(-\omega_3; \omega_L, \omega_L, -\omega_4) = \chi' + i\chi''$ responsible for the parametric process $\omega_L + \omega_L \rightarrow \omega_3 + \omega_4$. (a) Imaginary part of $\chi^{(3)}$; χ_I'' results from a single frequency resonance centered at $\omega_4 = \Omega_c$ (FWHM $= 2\Gamma_c$). χ_R'' is the contribution to χ'' from a difference frequency resonance centered at $\omega_L - \omega_4 = \Omega_b$ (FWHM $= 2\Gamma_b$). (b) Real part of $\chi^{(3)}$; χ_I' represents the contribution from a single frequency resonance. χ_R' originates from a difference frequency resonance. χ_{NR} is the non-resonant part of $\chi^{(3)}$ and is practically frequency independent.

$$\chi^{(3)}_{I,xxxx}(-\omega; \omega_L, \omega_L, \omega_\gamma) = \frac{NL e^4}{8\hbar^3} \sum_{\bar{c}} \frac{1}{\omega_{\bar{c}} - \omega_\gamma} \sum_{a,b} \langle g|x|a\rangle\langle a|x|b\rangle\langle b|x|\bar{c}\rangle\langle\bar{c}|x|g\rangle$$

$$\times \left[\frac{1}{(\omega_a - \omega)(\omega_b - \omega_L - \omega_\gamma)} + \frac{1}{(\omega_a^* + \omega_L)(\omega_b - \omega_L - \omega_\gamma)} + \frac{1}{(\omega_a^* + \omega_L)(\omega_b^* + 2\omega_L)}\right] \tag{29a}$$

$$\simeq \frac{NL e^4}{8\hbar^3} K' \sum_{\bar{c}} \langle g|x^3|\bar{c}\rangle\langle\bar{c}|x|g\rangle \left[\frac{\Omega_{\bar{c}} - \omega_\gamma}{(\Omega_{\bar{c}} - \omega_\gamma)^2 + \Gamma_{\bar{c}}^2} + \frac{i\Gamma_{\bar{c}}}{(\Omega_{\bar{c}} - \omega_\gamma)^2 + \Gamma_{\bar{c}}^2}\right]. \tag{29b}$$

K' is practically real and greater than zero. The slight frequency dependence of K' has been neglected. It can be shown that $\chi^{(3)}_{I,xxxx}(-\omega; \omega_L, \omega_L, \omega_\gamma)$ is approximately equal to $\chi_I^{(3)}(-\omega_\gamma; -\omega_L, -\omega_L, \omega)$. K' is approximately equal to $K/2$. As a result, $\chi^{(3)}_{I,xxxx}(-\omega; \omega_L, \omega_L, \omega_\gamma)$ and $\chi^{(3)}_{I,xxxx}(-\omega_3; \omega_L, \omega_L, -\omega_\gamma)$ are approximately equal.

In Fig. 3 the real and imaginary parts of $\chi^{(3)}_{xxxx}(-\omega; \omega_L, \omega_L, \omega_\gamma)$ are depicted for one single frequency resonance occuring at an energy state of frequency Ω_c.

3.4. Three-frequency mixing $\omega_L + \omega_L \pm \omega_R \rightarrow \omega$

3.4.1. Sum frequency generation $\omega_L + \omega_L + \omega_R \rightarrow \omega$

In the sum frequency process of Section 2.4.1. the coupling parameter is $\chi^{(3)}_{xxxx}(-\omega; \omega_L, \omega_L, \omega_R)$. This susceptibility is equal to $\chi^{(3)}_{xxxx}(-\omega; \omega_L, \omega_L, \omega_\gamma)$ of) of Section 3.3 with $\omega_\gamma = \omega_R$. In our experiments

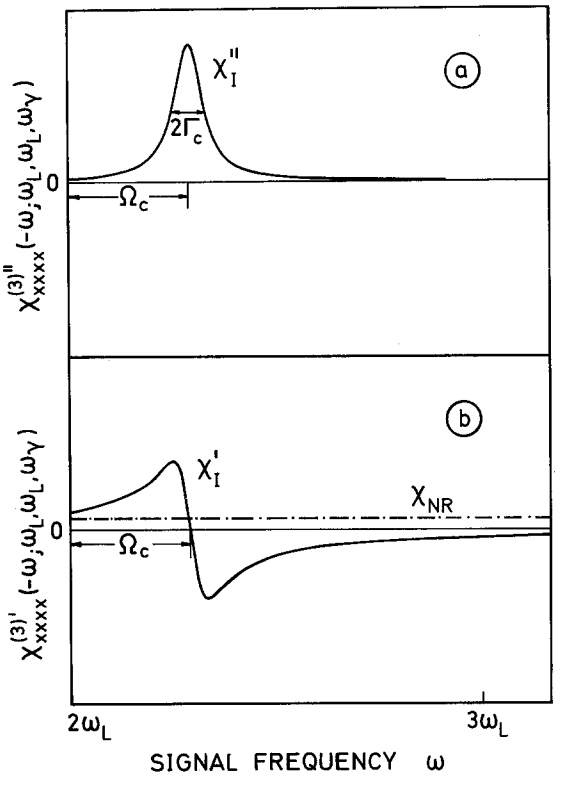

Figure 3 Schematic of the frequency dependence of the nonlinear susceptibility $\chi^{(3)}_{xxxx}(-\omega;\omega_L,\omega_L,\omega_\gamma)=\chi'+i\chi''$ which describes the frequency conversion process $\omega_L+\omega_L+\omega_\gamma\rightarrow\omega$.
(a) Imaginary part of $\chi^{(3)}$ resulting from a single frequency resonance centered at $\omega_\gamma=\Omega_c$ with half-width $2\Gamma_c$ (FWHM)
(b) Real part of $\chi^{(3)}$. The resonant part χ'_I is zero at $\omega_\gamma=\Omega_c$ and has its extrema at $\omega_\gamma=\Omega_c\pm\Gamma_c$. The nonresonant part χ_{NR} is frequency independent.

we consider only the situations where the light pulse at frequency ω_R is given by the first Stokes or anti-Stokes component generated by stimulated Raman scattering. In this case, ω_R is far away from vibronic resonances and no resonant terms are involved in $\chi^{(3)}_{xxxx}(-\omega;\omega_L,\omega_L,\omega_R)$.

3.4.2. Difference frequency generation $\omega_L+\omega_L-\omega_R\rightarrow\omega$

The difference frequency mixing process of Section 2.4.2. is described by the susceptibility $\chi^{(3)}_{xxxx}(-\omega;\omega_L,\omega_L,-\omega_R)$. This coupling term is equal to $\chi^{(3)}_{xxxx}(-\omega_3;\omega_L,\omega_L,-\omega_4)$ of Section 3.2. with $\omega_3=\omega$ and $\omega_4=\omega_R$. Here we are interested in the conversion of the Stokes light generated by stimulated Raman scattering into anti-Stokes light at $\omega=2\omega_L-\omega_R$. In this process ω_R the Stokes frequency is larger than the infrared absorption frequencies and the single frequency resonance terms are zero. The difference frequency resonance terms of Equation 27 are important; they are responsible for the strong Stokes–anti-Stokes coupling of the light waves (see Fig. 2 centre).

3.5. Third harmonic generation $\omega_L+\omega_L+\omega_L\rightarrow\omega$

The nonlinear susceptibility $\chi^{(3)}_{xxxx}(-\omega;\omega_L,\omega_L,\omega_L)$ is responsible for third harmonic generation. In our experiments with mode-locked Nd–glass lasers, the laser frequency $\omega_L/2\pi c=9455\,\mathrm{cm}^{-1}$ is well above the infrared absorption, i.e. no single frequency resonances at ω_L occur. Single frequency resonances at $\omega=3\omega_L$ and sum frequency resonances at $2\omega_L$ are absent in substances where the electronic absorption bands are in the ultraviolet region. In this case we have $\chi^{(3)}=\chi^{(3)}_{NR}$ $(D=1)$. In substances where $\omega=3\omega_L$ lies near an optical absorption band, third harmonic generation was not observed. The coherence length l_c is very short in these highly dispersive regions.

4. Experimental system

In our experiments we used a mode-locked Nd–glass laser [47, 48]. Single picosecond light pulses were selected from the mode-locked pulse train with an electro-optic shutter [49]. The energy of a

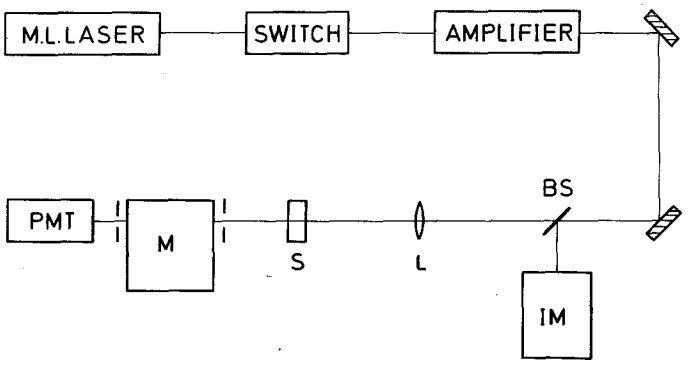

Figure 4 Experimental arrangement for measuring the spectral intensity distribution of the generated light. BS, beam splitter; IM, intensity detection; L, lens or inverted telescope; S, sample; M, monochromator; PMT, photomultiplier tube.

single light pulse was increased with the help of a laser amplifier. The amplified single light pulse had a duration of $\Delta t_L \simeq 6$ ps (FWHM) and a spectral width of $\Delta\tilde{\nu} \simeq 3\ \mathrm{cm}^{-1}$ (FWHM). These data indicate that single, nearly bandwidth limited light pulses were generated. The energy of the amplified pulse was approximately 5 mJ. The intensity of the light pulse in the sample was altered by filters, inverted telescopes or lenses. When telescopes or lenses ($f = 60$ cm and $f = 100$ cm) were used in the investigations of parametric four-photon processes, the sample was placed in a (slightly) divergent beam (after the focus of the lenses). The incident light intensity was determined by a saturable absorber system [50].

Experimentally we found new frequency components emitted in the forward direction within a divergence of $2\theta \simeq 4 \times 10^{-2}$ rad (measured at half maximum of the intensity). The generated light was found to be polarized parallel to the laser light. We verified in several substances (H_2O, D_2O, CH_2Cl_2, glass BK7, fused silica (Suprasil) and NaCl) that new light was emitted over a broad spectral region without self-focusing of the beam. The spectrum of the generated light was measured with a spectrograph and, simultaneously, the end face of the sample was investigated with a microscope and a photographic plate. No focal spots were observed in the magnified image of the exit window. In addition, visual inspection did not show breakdown sparks inside the medium.

The pulse duration of the parametric light in 2 cm of water was measured in the spectral range around $\lambda = 700$ nm with a picosecond streak camera (time resolution approximately 3 ps). The measurements were carried out at an input peak intensity of $I_{0L} \simeq 2 \times 10^{11}\ \mathrm{W/cm^2}$. The duration Δt_C of the generated pulse with broad spectrum was found to be slightly shorter than the laser pulse Δt_L with $\Delta t_C/\Delta t_L \simeq 0.8$.

The spectral distribution of the generated signal light was first observed qualitatively with a spectrograph and Polaroid films or spectroscopic plates. The intensity dependence of the spectral distribution was quantitatively studied with a double monochromator and photomultipliers. The experimental set-up for these measurements is shown schematically in Fig. 4. The parametrically generated idler light (on the Stokes side of the laser frequency) was measured with PbS-detectors and interference filters. The limited sensitivity of the infrared detector required relatively high input laser intensities close to the saturation range.

In our experiments a short sample length of 2 cm was used in general. With longer cells the interaction length for parametric light generation is limited by the different group velocities $v_g = c/[n - \lambda(\mathrm{d}n/\mathrm{d}\lambda)]$ of pump waves, signal and idler waves. The pump pulse and the generated pulse (6 ps duration) overlap for a travelled distance l_0 which is of the order of centimetres. In Fig. 5, calculated values of l_0 for a laser pulse at $\tilde{\nu}_L = 9455$ cm and a pulse at frequency $\tilde{\nu}$ are presented for water (pulse duration $\Delta t_L = 6$ ps). The effective interaction length z is limited to the overlapping length l_0.

5. Results

5.1. Water

First we discuss experimental and theoretical results obtained for water (cell length 2 cm). The Raman susceptibility χ''_R [51, 52, 38] and the nonlinear refractive index n_2 [18, 19, 54–56] (at $\tilde{\nu}_L = 9455\ \mathrm{cm}^{-1}$) are small in water. Difference frequency resonances of $\chi^{(3)}$ and the resulting light generation by stimu-

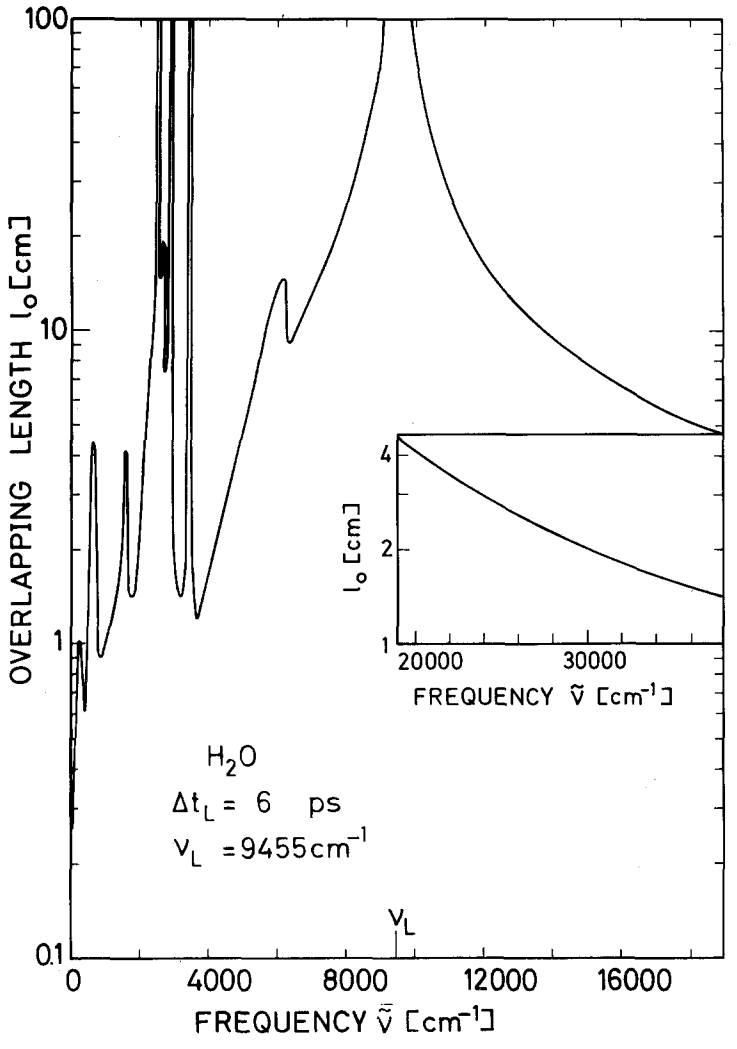

Figure 5 Spatial overlap l_0 between a laser pulse of duration $\Delta t_L = 6$ ps and a spectral component at frequency $\tilde{\nu}$ (Substance: water). l_0 is defined as the path-length that produces a delay of $\Delta l = \Delta t_L \times c/n$ between the pulse at frequency $\tilde{\nu}_L$ and the pulse at frequency $\tilde{\nu}$.

lated Raman scattering do not – at the beginning – effect the parametric four-photon processes. These facts simplify our analysis. The small value of n_2 excludes self-focusing and makes the spectral broadening due to self-phase modulation very small at our laser frequency.

We measured the energy conversion (per frequency interval) of laser into signal light at ν_3 as a function of input peak intensity I_{0L} for a number of frequencies in the range between 200 nm and 925 nm. As an example, experimental data are presented for three frequencies at 13 700, 14 900, and 23 800 cm^{-1} in Fig. 6. The energy conversion per wave number $\eta(\tilde{\nu}) = \int \epsilon(\tilde{\nu})\, dA/W_L$ (W_L is the energy of the laser pulse, dA represents a cross-sectional element) increases very rapidly for all frequencies. Values of $\eta(\tilde{\nu})$ rise by a factor of 10^5, when the input peak intensity is increased by approximately a factor of two. The results of Fig. 6 demonstrate quite vividly rapid growth (high gain) of the generation process. For $I_{0L} \gtrsim 5 \times 10^{10}$ W/cm^2 saturation sets in.

5.1.1. Frequency range between ω_L and $2\omega_L$

We begin the discussion of our investigations in the frequency range between ω_L and $2\omega_L$ [8]. In Fig. 7, the energy conversion is depicted over the frequency range from 10 800 cm^{-1} to $2\tilde{\nu}_L = 18\,910$ cm^{-1}. Five curves for different input peak intensities are presented (they are derived for each frequency from data such as depicted in Fig. 6). At $I_{0L} \simeq 2 \times 10^{10}$ W/cm^2 the parametrically generated light starts at

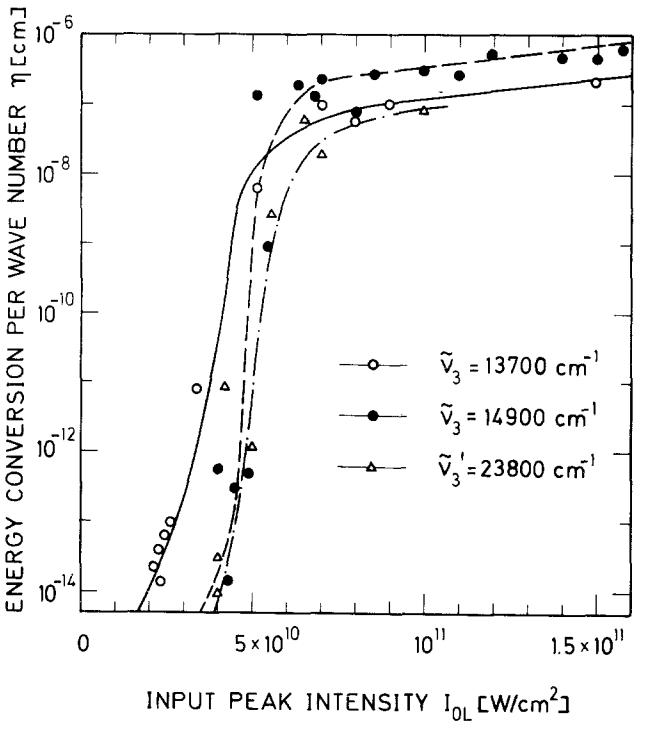

Figure 6 Energy conversion η of laser light ($\tilde{\nu}_L = 9455\,cm^{-1}$) into short-wavelength radiation at $\tilde{\nu}_3$ (substance: water). The curves below saturation are calculated. At $\tilde{\nu}_3 = 13\,700\,cm^{-1}$ and $14\,900\,cm^{-1}$ the parametric process $\omega_L + \omega_L \rightarrow \omega_3 + \omega_4$ is considered. $\chi^{(3)}$ values are taken from Fig. 10. At $\tilde{\nu} = 23\,800\,cm^{-1}$ the dash-dot line below $I_{0L} = 5 \times 10^{10}\,W/cm^2$ is calculated for the frequency conversion process $\omega_L + \omega_L + \omega_\gamma \rightarrow \omega$ with $\chi^{(3)}$ taken from Fig. 14.

discrete frequencies far away from the laser intensity. With increasing input intensity the energy conversion at fixed frequencies increases approximately exponentially (See Fig. 6). Up to $I_{0L} \simeq 5 \times 10^{10}\,W/cm^2$ the spectrum broadens but a certain degree of the structure of the spectral distribution persists. At input intensities $\gtrsim 10^{11}\,W/cm^2$ a rather smooth spectral distribution is obtained. The follow-

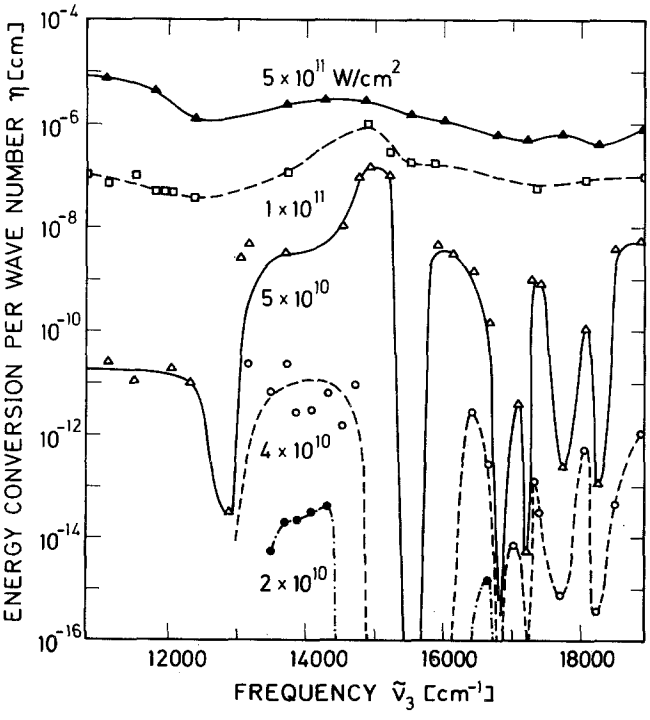

Figure 7 Experimental energy conversion η versus signal frequency $\tilde{\nu}_3$ ($10\,800\,cm^{-1} \leqslant \tilde{\nu}_3 \leqslant 2\tilde{\nu}_L$) in water for five laser input peak intensities.

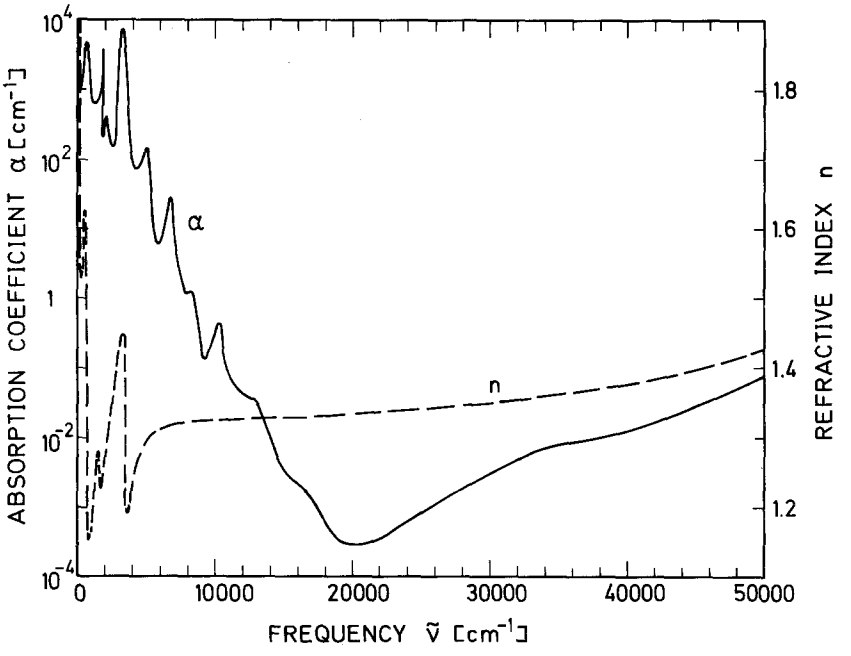

Figure 8 Linear absorption coefficient α [58, 59] and refractive index n [57] of water.

ing calculations show that the light generated at $I_{0L} \lesssim 5 \times 10^{10}\text{W/cm}^2$ is due to the parametric four-photon process $\omega_L + \omega_L \rightarrow \omega_3 + \omega_4$. The signal light formed in this primary parametric four-photon process acts as a pump wave in secondary parametric processes. These subsequent parametric processes are of the form $\omega_L + \omega_3 \rightarrow \omega_3' + \omega_4'$; they flatten the spectrum at higher intensities. For these processes Δk is small and $\chi^{(3)}$ is enlarged by difference frequency resonances ($\omega_3 - \omega_3'$ and $\omega_4' - \omega_L$ or $\omega_3' - \omega_3$ and $\omega_L - \omega_4'$ nearly equal to Ω_b). The onset of secondary and higher order parametric processes removes energy from the frequency range of the primary process. Together with the depletion of the peak intensity of the laser pulses, they lead to a saturation of the energy conversion η. The situation of parametric light generation at high input intensities will be discussed in more detail below.

In the intensity range $I_{0L} \lesssim 5 \times 10^{10}\text{W/cm}^2$ we consider the four-photon parametric process $\omega_L + \omega_L \rightarrow \omega_3 + \omega_4$. The spectral energy density of Equation 10a and the energy conversion efficiency η of Fig. 7 are related by Equation 30:

$$\eta(\tilde{\nu}_3) = \frac{\int \epsilon(\tilde{\nu}_3)\,\mathrm{d}A}{W_L} = \frac{\epsilon(\tilde{\nu}_3) d_3^2}{I_{0L}\Delta t_L d_L^2}. \tag{30}$$

Numerical estimates indicate that the beam diameter of the generated light d_3 is approximately one-fifth of the laser beam diameter d_L. From our experimental data of Fig. 7 we determine the frequency dependence of the nonlinear susceptibility $\chi^{(3)} = 3\chi_{NR} + \chi_I + \chi_R = \chi^{(3)\prime} + i\chi^{(3)\prime\prime}$. The various parameters which enter Equations 10a and 30 are measured directly (I_{0L}, Δt_L, d_L), or are taken from the literature (α_i; n_i, Δk).

In Fig. 8 literature data for the dispersion of the refractive index [57] and of the absorption coefficient [58, 59] are presented. The linear absorption of water is very large in the infrared resulting in considerable variations of the refractive index. In the visible and ultraviolet region, the absorption is small and the refractive index changes only slightly.

Fig. 9 shows the calculated phase-mismatch $\Delta k = k_3 + k_4 - 2k_L$ for collinear light interactions and the phase-matching angles for non-collinear light interactions with $\Delta k = 0$ [60, 61]. At certain frequencies the phase-matching angles are larger than the measured divergence of the beam ($\theta \simeq 2 \times$

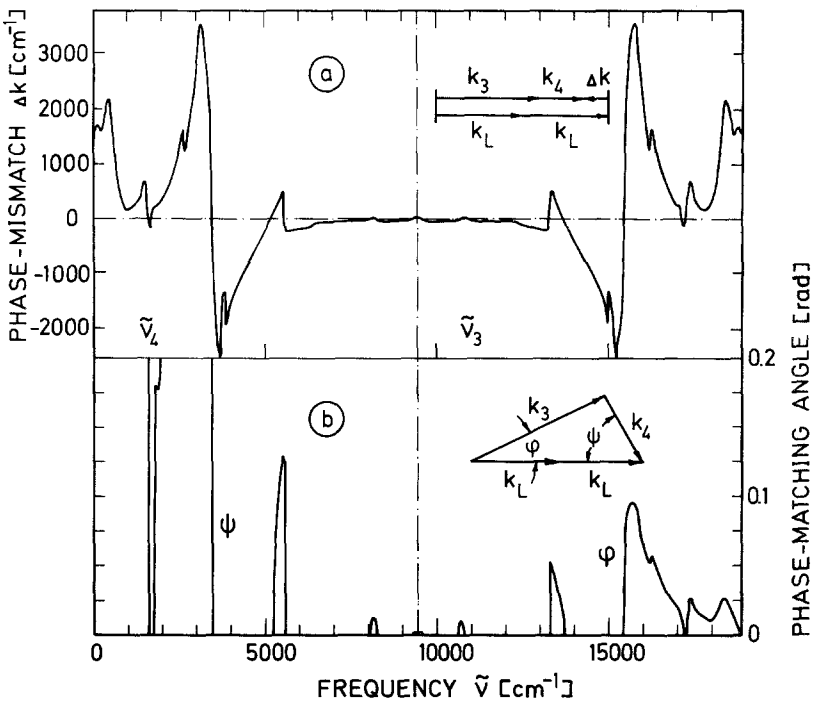

Figure 9 (a) Collinear phase-mismatch $\Delta k = k_3 + k_4 - 2k_L$ and (b) noncollinear phase-matching angles ϕ and ψ for the interaction $\omega_L + \omega_L \rightarrow \omega_3 + \omega_4$ (substance: water).

10^{-2} rad, at half intensity value); in other frequency regions perfect phase-matching ($\Delta k = 0$) is impossible. As a result, the parametric generation process proceeds in certain frequency regions with a well-defined phase-mismatch. Equation 10a applies to collinear light generation, but it represents a good approximation for small divergence angles. For collinear light beams the interaction length between signal, idler and pump wave is given by the length of the cell (or by the overlapping length l_0 of Fig. 5). For non-collinear phase-matching the interaction length is strongly reduced due to the large walk-off angle of the light (see insert in Fig. 9b).

The nonlinear susceptibility $\chi^{(3)}(-\omega_3, \omega_L, \omega_L, -\omega_4) = \chi^{(3)\prime} + i\chi^{(3)\prime\prime}$ represents a complex quantity; it cannot be determined completely by fitting Equation 10a to the experimental data. We take advantage of our knowledge concerning the frequency distribution of $\chi^{(3)\prime\prime} = \chi''_R + \chi''_I$ and we use the relations between the real and the imaginary parts of $\chi^{(3)}_R$ and $\chi^{(3)}_I$ developed in Section 3. Fig. 10 depicts the results of our analysis. Fig. 10a shows the imaginary part of $\chi^{(3)}$. χ''_R was obtained from Raman data [51–53]. A frequency corrected Raman gain factor of $g_S = (64\pi^3 \tilde{\nu}_S/(n_S n_L c))\chi''_R(\bar{\Omega}_b) \simeq 7 \times 10^{-11}$ cm/W is deduced from the literature [51–53] for the vibrational mode at $\tilde{\nu}_{vib} = \bar{\Omega}_b/2\pi \simeq 3300\,\text{cm}^{-1}$; the peak Raman susceptibility has a value of $\chi''_R(\bar{\Omega}_b) = 3 \times 10^{-14}\,\text{cm}^3/\text{erg}$. The frequency distribution of $\chi^{(3)\prime\prime}_{I,xxxx}(-\omega_3; \omega_L, \omega_L, -\omega_4)$ is chosen to be proportional to the absorption $-\alpha(\omega_4)$ as discussed in Section 3. The full curve in Fig. 10b shows the real part $\chi^{(3)\prime}_{xxxx}(-\omega_3; \omega_L, \omega_L, -\omega_4) = 3\chi_{NR} + \chi'_I + \chi'_R$. The value of $3\chi_{NR} \simeq 2 \times 10^{-14}\,\text{cm}^3/\text{erg}$ is taken from the literature [18, 19]. χ'_I and χ'_R were calculated from the imaginary parts using the relation of Equations 26 and 28. The absolute scale of χ''_I is determined from the experimentally measured energy conversions in the range between 14 300 cm^{-1} and 15 200 cm^{-1}. The other points in Fig. 10b are determined from Equation 10a by using the curve of $\chi^{(3)\prime\prime}$ of Fig. 10a and the experimentally measured energy conversion data of Fig. 7. The good agreement between the experimental points and the $\chi^{(3)\prime}$-curve over the large frequency range should be noted.

The real part of the Raman susceptibility $\chi^{(3)}_R$ around 12 900 cm^{-1} is smaller by approximately a factor of ten than the nonlinear susceptibility $\chi^{(3)\prime}_I$ (12 900 cm^{-1}) originating from infrared resonances.

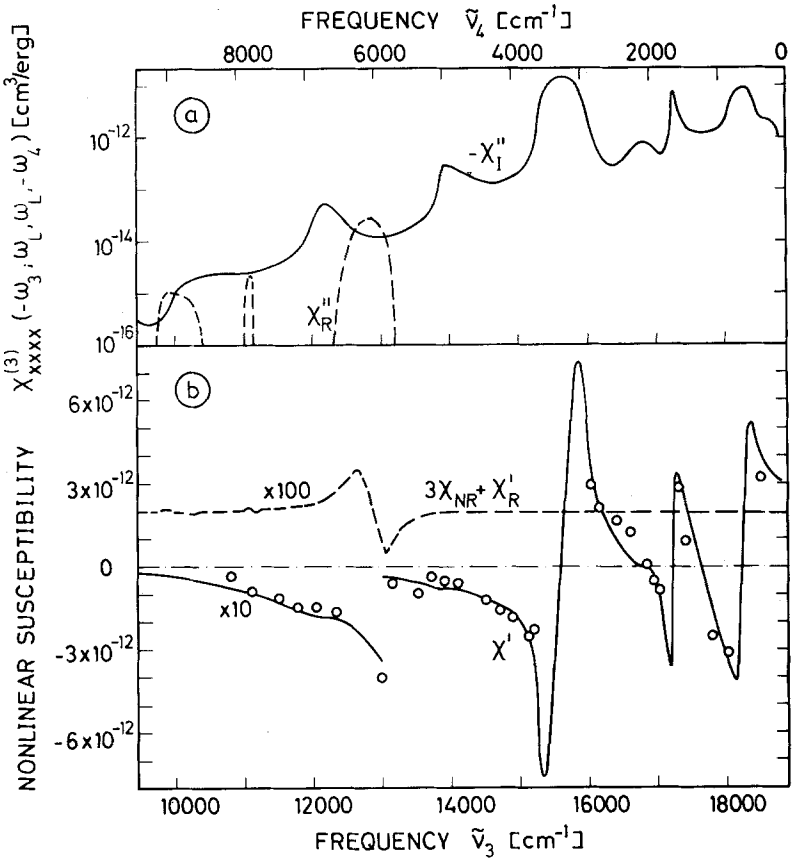

Figure 10 Nonlinear susceptibility $\chi^{(3)}_{xxxx}(-\omega_3;\omega_L,\omega_L,-\omega_4)$ of water. (a) Imaginary parts χ_I'' and χ_R''; χ_I'' is obtained from the absorption spectrum $\alpha\cdot\chi_R''$ is taken from Raman data [51–53]. (b) Total real part $\chi' = 3\chi_{NR} + \chi_I' + \chi_R'$ and magnified components $3\chi_{NR} + \chi_R'$; ($3\chi_{NR} \simeq 2 \times 10^{-14}$ cm^3/erg [18, 19]. The structure of χ_R' and χ_I' is obtained from Equations 28 and 26. The absolute scale is calculated from Equation 10a using experimental data around $\tilde{\nu} = 15\,000\,\text{cm}^{-1}$. Open circles, experimental points.

The parametric light generated by Raman resonances is negligible compared to the light generation by infrared resonances.

It is interesting to see that the three major infrared peaks of water at 650, 1600 and 3300 cm^{-1} give rise to single frequency resonances in $\chi_I^{(3)}$ and cause large values of the imaginary part $\chi_I^{(3)\prime\prime}$ over a wide range of signal frequencies ν_3. Five minima of the energy conversion curves of Fig. 7 ($I_L < 1 \times 10^{11}$ cm^2) are accounted for by the three major maxima of χ_I'' at $\tilde{\nu}_3 = 18\,250$, 17 250, 15 600 cm^{-1} where $\chi_I' \simeq 0$ and by the change in sign of χ_I' between resonances at $\tilde{\nu}_3 = 17\,650$ and 16 800 cm^{-1}. The sixth minimum in the spectral distribution of η at $\tilde{\nu}_3 \simeq 12\,900$ cm^{-1} results from inverse Raman scattering [90]. Light generated by parametric four-photon interaction at $\omega_3 = \omega_L + \omega_{vib}$ is converted back to the pump frequency ω_L and to the vibrational excitation at ω_{vib}. The loss of spectral energy density is estimated below; it agrees with the experimental observation.

From the detailed agreement between theory and experiment we conclude that the signal light between ω_L and $2\omega_L$ is produced by the parametric four-photon process $\omega_L + \omega_L \rightarrow \omega_3 + \omega_4$ (for $I_0 \lesssim 5 \times 10^{10}$ W/cm^2).

5.1.2. *Frequency range below* ω_L

At low laser intensities the idler generation (process $\omega_L + \omega_L \rightarrow \omega_3 + \omega_4$) was estimated from the signal light using Equations 10a and b. The relation between idler and signal light is given by:

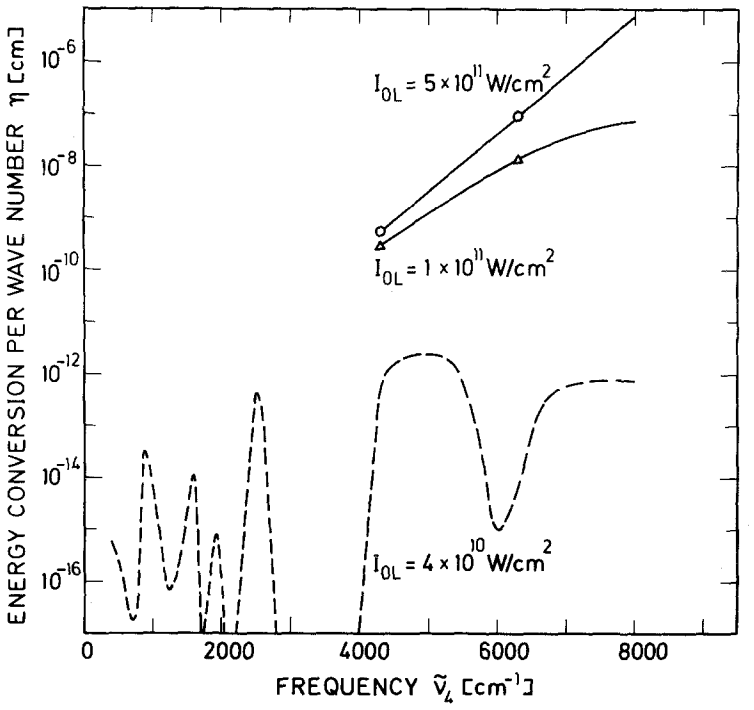

Figure 11 Calculated energy conversion η versus idler frequency $\tilde{\nu}_4$ (infrared) at $I_{0L} = 4 \times 10^{10}$ W/cm^2 and measured energy conversion at $I_{0L} = 10^{11}$ W/cm^2 and 5×10^{11} W/cm^2

$$I(\omega_4) = I(\omega_3)(\omega_4/\omega_3)(n_3/n_4)^3 \tag{31}$$

when no depletion of the laser light occurs (the same relation applies to the energy conversions). In Fig. 11 the calculated energy conversion at $I_L = 4 \times 10^{10}$W/cm^2 is presented; it reflects the strong single frequency resonances discussed in connection with the frequency dependence of the signal output.

In Fig. 11 several experimental points of the idler energy conversion are shown for high laser intensities of $I_L = 1 \times 10^{11}$ and 5×10^{11}W/cm^2. Comparison of the measured idler with the corresponding signal output shows a drastic reduction of the idler light. For instance, the energy conversion per wave number η has values of 10^{-10} and 10^{-7} at $\tilde{\nu}_4 = 4000\,\text{cm}^{-1}$ and $\tilde{\nu}_3 = 14\,000\,\text{cm}^{-1}$, respectively, ($I_L = 1 \times 10^{11}$W/cm^2). This effect is due to the strong infrared absorption at the idler frequencies as demonstrated by the numerical calculations of Fig. 1b.

The parametric frequency down conversion process [22] $\omega_L \rightarrow \omega_{i1} + \omega_{i2} + \omega_{i3}$ would produce light components on the Stokes side of the laser frequency. This process was not discussed theoretically in Sections 2 and 3. The amplifaction factor $gg^*\chi^2$ of this process compared to the process $\omega_L + \omega_L \rightarrow \omega_3 + \omega_4$ (Equation 9d) is given by:

$$\frac{(gg^*\chi^2)(\omega_L \rightarrow \omega_{i1} + \omega_{i2} + \omega_{i3})}{(gg^*\chi^2)(\omega_L + \omega_L \rightarrow \omega_3 + \omega_4)} \simeq \frac{I_{IR}\chi^{(3)}(-\omega_{i3}; \omega_L, -\omega_{i1}, -\omega_{i2})^2}{I_L\chi^{(3)}(-\omega_3; \omega_L, \omega_L, -\omega_4)^2} \tag{32}$$

I_{IR} is given by the intensity of the quantum fluctuations and is about ten orders of magnitude less intense than I_L, when frequency down conversion without infrared input pulses at ω_{i1}, ω_{i2} or ω_{i3} is considered. $\chi^{(3)}(-\omega_{i3}; \omega_L, -\omega_{i1}, -\omega_{i2})$ may possess two resonance terms within one denominator of Equation 25, so that an increase of $\chi^{(3)}(-\omega_{i3}; \omega_L, -\omega_{i1}, -\omega_{i2})$ by a factor of hundred compared to $\chi^{(3)}(-\omega_3; \omega_L, \omega_L, -\omega_4)$ is possible. At these frequencies two infrared light frequencies are strongly absorbed and the threshold for parametric amplification increases correspondingly. Without input pulses at ω_{i1}. ω_{i2}, or ω_{i3} the frequency down conversion process does not play any role [62–64]. Even at high laser intensities of about 2×10^{11}W/cm^2, where parametric processes have produced a total energy conversion of about 10^{-4} on the Stokes side of the laser frequency, the frequency down conversion process

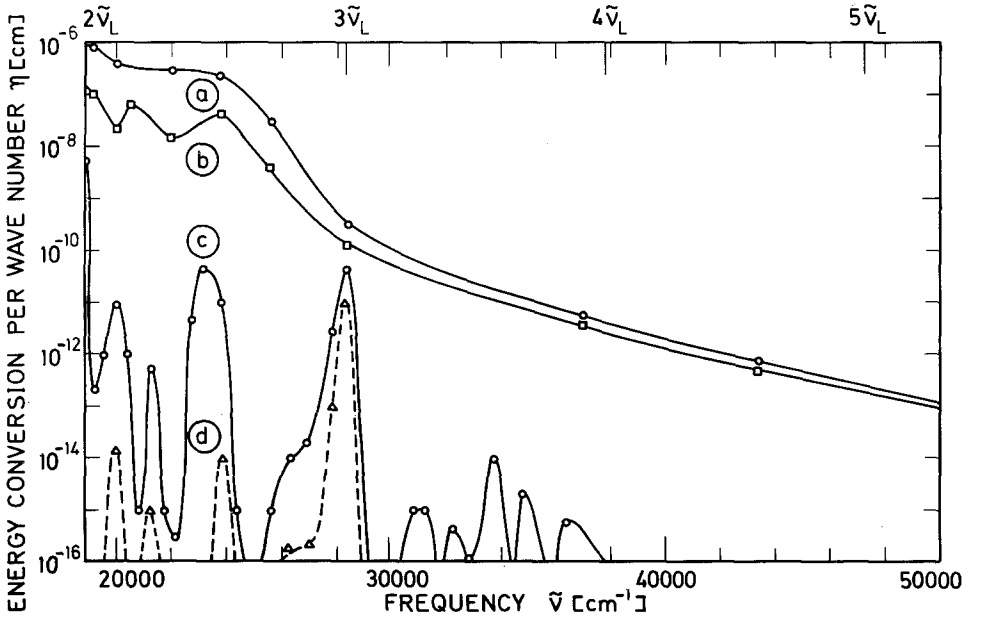

Figure 12 Experimental energy conversion η per wave number interval versus frequency $\tilde{\nu}$ for four laser input peak intensities: (a) 5×10^{11}; (b) 1×10^{11}; (c) 5×10^{10}; (d) 4×10^{10} W/cm^2. Substance: water.

seems to be small. At very high laser intensities, this process may contribute to the reduction of the total light output by transfer of laser light to the infrared region and strong infrared absorption.

5.1.3. Frequency range beyond $2\omega_L$

The measured energy conversion efficiency η in the frequency range between 18 900 cm^{-1} and 50 000 cm^{-1} is depicted in Fig. 12 for four laser intensities, 4×10^{10} W/cm^2, 5×10^{10} W/cm^2,

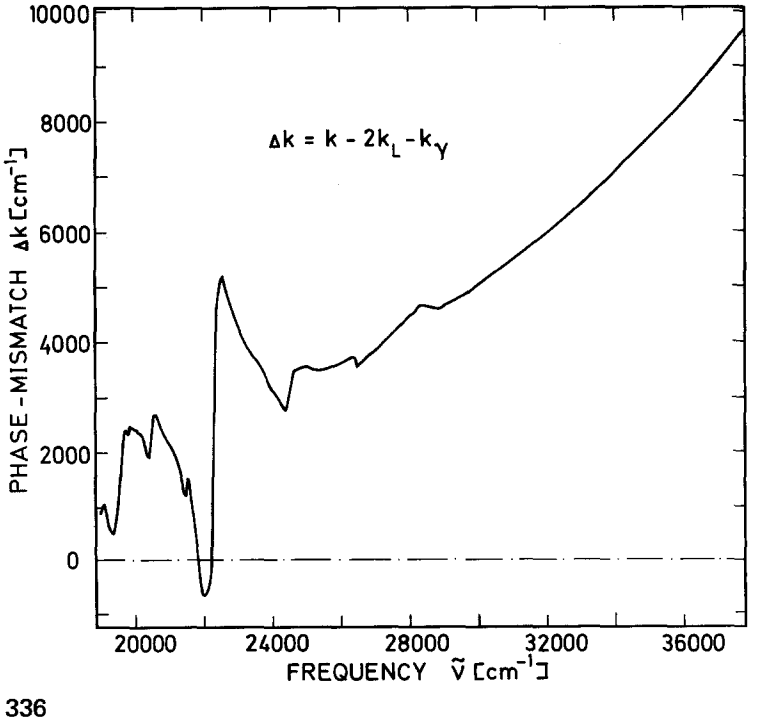

Figure 13 Calculated collinear phase mismatch $\Delta k = k - 2k_L - k_\gamma$ for the interaction process $\omega_L + \omega_L + \omega_\gamma \rightarrow \omega$ ($0 \leq \omega_\gamma \leq 2\omega_L$). Substance: water.

10^{11} W/cm^2, and 5×10^{11} W/cm^2. At the smallest input intensity of $I_{0L} = 4 \times 10^{10}$ W/cm^2, parametric light was detected in small frequency regions. At $I_{0L} = 5 \times 10^{10}$ W/cm^2, the energy conversion increased strongly and extended over a larger frequency range. At $I_{0L} > 10^{11}$ W/cm^2, some structure remains in a broad spectrum. In the range from 19 000 cm^{-1} to 26 000 cm^{-1}, the energy conversion has values of approximately 5×10^{-7}/cm^{-1}. For larger frequencies the energy conversion decreases continuously to $\eta \simeq 10^{-13}$ cm at $\tilde{\nu} = 50\,000$ cm^{-1}.

At the third harmonic frequency $\omega = 3\omega_L$, light could be detected at input intensities as low as $I_{0L} = 5 \times 10^9$ W/cm^2. Inserting the parameters $\omega/2\pi c = 28\,365$ cm^{-1}, $n = 1.35$, $n_L = 1.33$, $\chi^{(3)}_{NR} = (2/3) \times 10^{-14}$ cm^3/erg, and $\Delta k = 4600$ cm^{-1} into Equation 22 we calculate a maximum intensity conversion efficiency of $I/I_L \simeq 2 \times 10^{-28} I_L^2$ (I and I_L in units of W/cm^2). The energy conversion efficiency is estimated to be $\eta_{3\omega_L} = \int I(r, t) r \, dr \, dt / \int I_L(r, t) r \, dr \, dt \simeq 2 \times 10^{-28} \int I_L^3(r, t) r \, dr \, dt / \int I_L(r, t) r \, dr \, dt \simeq 10^{-30} I_{0L}^2$. At $I_{0L} = 5 \times 10^{10}$ W/cm^2, a maximum energy conversion of $\eta_{3\omega_L} \simeq 3 \times 10^{-9}$ is expected. Experimentally, an energy conversion per wave number of approximately 5×10^{-11}/cm^{-1} was found. Multiplying this value by the system resolution of about 100 cm^{-1} (at this wave-length) we obtain an experimental value of $\eta_{3\omega} \simeq 5 \times 10^{-9}$. The measured and the calculated numbers are in good agreement.

For a discussion of the generated broad spectra we consider two parametric processes: (i) frequency up-conversion $\omega_L + \omega_L + \omega_\gamma \rightarrow \omega$ and (ii) secondary parametric interactions $\omega_L + \omega_3 \rightarrow \omega_3' + \omega_4'$, $(\omega_3 > \omega_L)$.

(i) In the frequency conversion process, parametric light which was generated in the primary four photon process ($\omega_L + \omega_L \rightarrow \omega_3 + \omega_4$) is converted to higher frequencies $\omega > 2\omega_L$. The detailed structure in the emitted spectrum for laser intensities $I_{0L} \lesssim 5 \times 10^{10}$ W/cm^2 allows us to state unambiguously that this parametric process occurs under our experimental conditions (see Fig. 12).

The frequency to be converted is denoted by ω_γ. Primary signal light (ω_3) produces light in the frequency range $3\omega_L < \omega < 4\omega_L$, while primary idler waves (ω_4) generate light frequencies $2\omega_L < \omega < 3\omega_L$. The spectral distributions of the input pulses $I(\omega_\gamma, 0)$ are obtained from Fig. 7 and 11 (together with Equation 30) for signal and idler, respectively.

The spectral intensity $I(\omega)$ or the energy conversion $\eta(\omega)$ which is generated in the frequency conversion process, can be calculated with the help of Equation 18. For a quantitative evaluation we have to know $\epsilon(\omega_\gamma, 0)$, α, n, Δk and $\chi^{(3)}$. Since the input light $\epsilon(\omega_\gamma, 0)$ is generated in the first part of the medium, the frequency conversion process takes place at the end of the light path through the sample. In our calculations we take for $\epsilon(\omega_\gamma, 0)$ the spectral energy density of the signal and idler at the end of the cell. The interaction length is assumed to be approximately 0.5 cm. The values of α and n are obtained from Fig. 8. The phase mismatch $\Delta k = k - 2k_L - k_\gamma$ is calculated from the colour dispersion of Fig. 8 and presented in Fig. 13 for the frequency range of 18 900 cm^{-1} to 37 800 cm^{-1}. We note a substantial phase mismatch in particular for frequencies exceeding 22 000 cm^{-1}. The nonlinear susceptibility of our frequency conversion process $\chi^{(3)}_{xxxx}(-\omega; \omega_L, \omega_L, \omega_\gamma)$ contains terms with single frequency resonances but has no contributions with difference frequency denominators. The imaginary part of χ^3 has the form $\chi^{(3)\prime\prime}(-\omega; \omega_L, \omega_L, \omega_\gamma) = \chi_I^{(3)\prime\prime}(-\omega; \omega_L, \omega_L, \omega_\gamma) \simeq -\chi_I^{(3)}(-\omega_3; \omega_L, \omega_L, -\omega_\gamma)$. The real part of the single frequency resonant terms is analogous to the primary parametric process. The non-resonant part of χ^3 is assumed to be constant with the value quoted above. In Fig. 14 the imaginary and real parts of $\chi^{(3)}$ are plotted as a function of frequency. The single frequency resonances lead to strong fluctuations of the $\chi^{(3)}$ values, suggesting maxima and minima in the frequency conversion process. For frequencies exceeding 26 000 cm^{-1} we find small values of $\chi^{(3)}$. Using Equations 18 and 30 we calculated the energy conversion for two laser intensities $I_{0L} = 4 \times 10^{10}$ and 5×10^{10} W/cm^2; the respective data are depicted in Figs. 15a and b. Of interest is the comparison between the measured and calculated energy conversion of Fig. 12 and Fig. 15, respectively. The numerous minima and the order of magnitude of the maxima are well accounted for by our calculations. We wish to conclude that frequency conversion contributes significantly to the parametric light observed at frequencies between $2\omega_L$ and $4\omega_L$.

(ii) Secondary parametric processes of the type $\omega_L + \omega_3 \rightarrow \omega_3' + \omega_4'$ are discussed next. When the

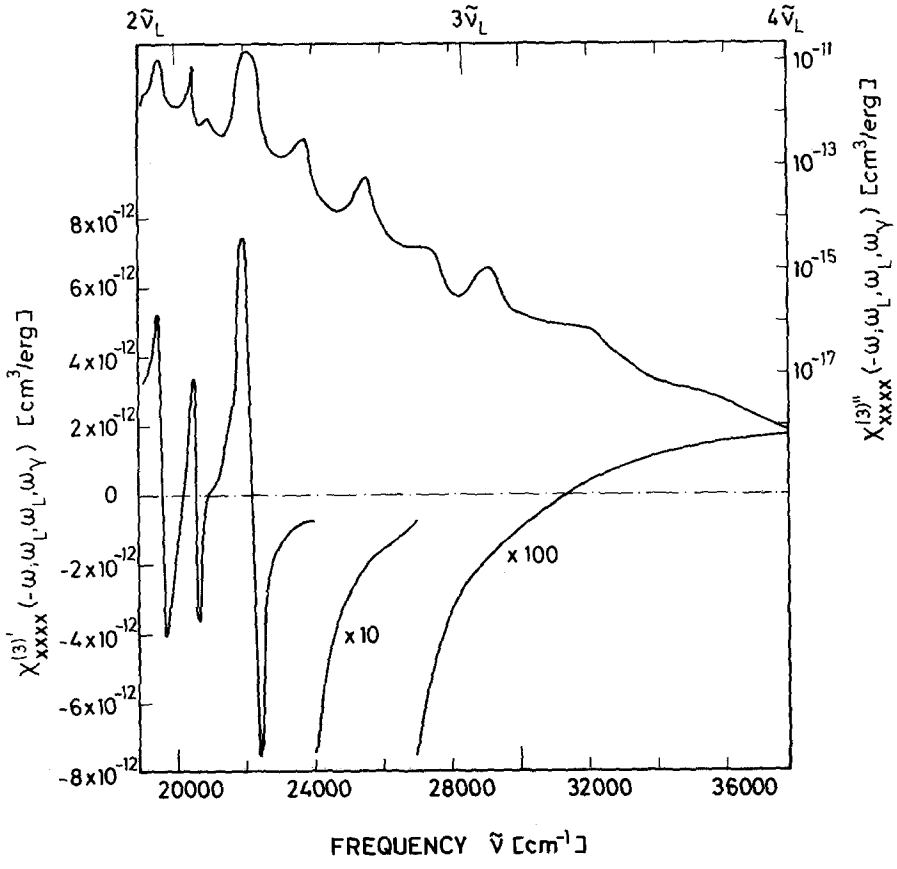

Figure 14 Nonlinear susceptibility $\chi^{(3)}_{xxxx}(-\omega;\omega_L,\omega_L,\omega_\gamma)$ of water. For $0 \leqslant \omega_\gamma \leqslant \omega_L$, $\chi^{(3)}$ is taken from Fig. 10 since $\chi^{(3)}(-\omega;\omega_L,\omega_L,\omega_\gamma) \simeq \chi^{(3)*}(-\omega_3;\omega_L,\omega_L,-\omega_\gamma)$. For $\omega_L < \omega_\gamma \leqslant 2\omega_L$, the χ'' and χ' curves are extended using the proportionality between $\chi^{(3)}$ and α.

broad band signal pulse (ω_3) of the primary process $\omega_L + \omega_L \rightarrow \omega_3 + \omega_4$ acts as one of the two pump pulses, new frequencies (ω_3') between $2\omega_L$ and $3\omega_L$ are expected. Two points should be noted here. First, various parts of the broad input signal contribute to the output at a certain frequency ω_3' and second, the spectral intensity of the idler in the primary process provides the initial condition for the secondary process, i.e., $I_N(\omega_4)$ of Equation 10a has to be replaced by $I(\omega_4, l)$. To evaluate the output intensity at ω_3', the broad input spectrum was subdivided into a number of frequency intervals and the contributions added for the secondary process. By this method we find a very small energy conversion of $\eta(\omega_3') < 10^{-18}$ cm for $I_{0L} \lesssim 4 \times 10^{10}$ W/cm^2. In Fig. 15b, the calculated energy conversions $\eta(\omega_3')$ are shown for $I_{0L} = 5 \times 10^{10}$ W/cm^2. For larger laser intensities the efficiency of the secondary parametric process rises very quickly since the parametrically produced pump pulse approaches the peak intensity of the laser pulse. We point to Figs 7 and 12 where a conversion efficiency per wave number of $\eta \simeq 10^{-7}$ cm is observed over a large spectral range of approximately 15 000 cm^{-1} ($I_{0L} = 10^{11}$ W/cm^2). Under these conditions a total energy conversion of $\eta_t \simeq 1.5 \times 10^{-3}$ (see Fig. 16) and a total intensity conversion of 10^{-1} is estimated.

5.1.4. Saturation of light generation

We have measured the total energy conversion and the energy transmission of the incident pulse at very high light intensities. Our measurements and our calculations indicate that at $I_{0L} \gtrsim 10^{11}$ W/cm^2 parametric light is generated over a broad spectral range which extends from the ultraviolet to the absorbing infrared

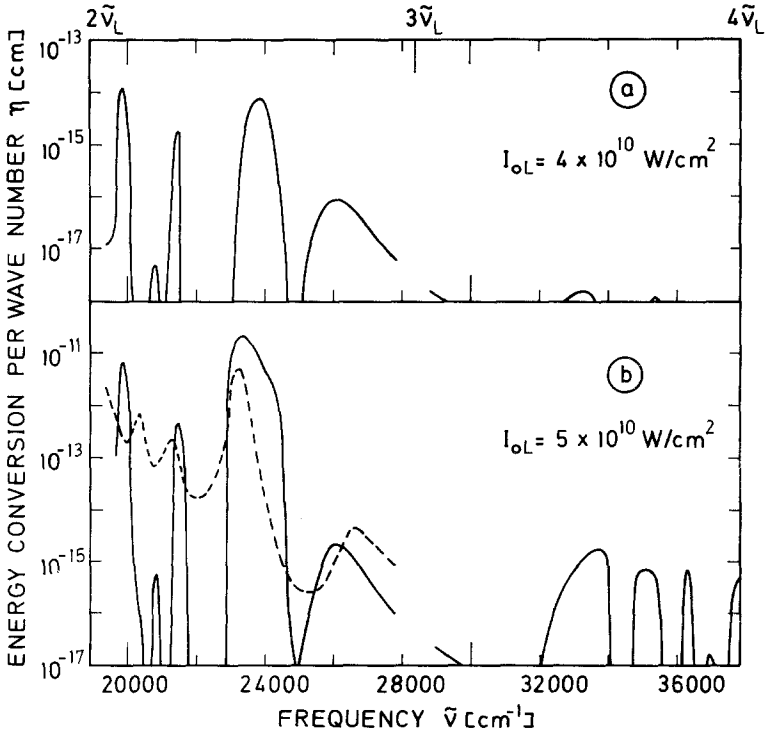

Figure 15 (a) Calculated energy conversion η for the process $\omega_L + \omega_L + \omega_\gamma \rightarrow \omega$ at an input laser peak intensity of $I_{0L} = 4 \times 10^{10}$ W/cm².
(b) Calculated energy conversion $I_{0L} = 5 \times 10^{10}$ W/cm². The frequency conversion process $\omega_L + \omega_L + \omega_\gamma \rightarrow \omega$ (solid curve) and the secondary parametric process $\omega_L + \omega_3 \rightarrow \omega_3' + \omega_4'$ (dashed curve) are depicted.

region. As soon as the laser light is depleted, the parametric light generation is reduced and the generated idler light becomes strongly absorbed in the infrared region. Input energy is continuously lost by idler absorption. In Fig. 16 the total parametric light output over the whole spectral range and the transmission of the laser pulse are shown for the case of water. At high laser intensities a total energy con-

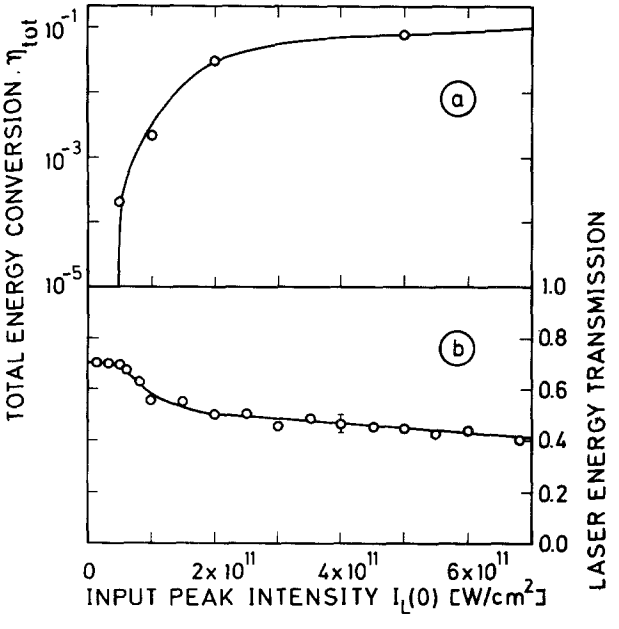

Figure 16 (a) Total energy conversion of laser light into parametric light.
(b) Energy transmission of the laser pulse versus input peak intensity. Single picosecond light pulses ($\lambda = 1.06\,\mu$m) of $\Delta t_L \simeq 6$ ps traversed 2 cm of water.

version of up to 10% could be obtained. The laser transmission is reduced from its linear transmission value of 0.7 at 9455 cm^{-1} to a value of 0.4. The increased loss of laser light is explained by energy transfer to the strongly absorbed idler waves (see numerical results of Fig. 1).

In the ultraviolet region the parametric light generation is small. The large phase-mismatch due to the strong dispersion of the refractive index lowers the frequency conversion efficiency. In addition, the conversion efficiency of the parametric processes is reduced with increasing order.

5.2. Other substances

Broad emission spectra were observed in a number of materials. In D_2O, NaCl and quartz glass, emission spectra extended to 200 nm and values for the total energy conversion similar to H_2O were measured. In NaCl and quartz glass (Infrasil) the laser peak intensity had to be kept below $I_{0L} \simeq 3 \times 10^{11}$ W/cm^2 in order to avoid self-focusing and damage. In substances with optical absorption in the range between 200 and 400 nm ($C_6H_5NO_2$, CS_2, CH_2I_2, CH_3COCH_3, CH_3CCl_3, CH_2Cl_2, CH_2Cl_2, CH_3CH_2OH, glasses BK7 and SF59) the emission extended to frequency values near the absorption bands (see also [4]). High linear absorption and large phase-mismatch prevent parametric light generation at shorter wave lengths. Two and three photon absorption processes reduce the parametric light output near the absorption bands [15].

In substances without idler absorption (e.g. NaCl) and with reduced colour dispersion the nonresonant susceptibility is sufficient for efficient light generation (see estimates following Equation 13).

In all materials which do not absorb at $\omega = 3\omega_L$ (e.g. H_2O, D_2O, CH_3COCH_3, CH_3CCl_3, CCl_4, CH_3CH_2OH, glass BK7, quartz glass Suprasil and NaCl) third harmonic generation was readily observed with a double monochromator and photomultiplier or with a spectrograph and Polaroid films. Substances which absorb at $\omega = 3\omega_L$ (e.g. $C_6H_5NO_2$, CS_2, CH_2I_2 and glass SF59) did not show detectable third harmonic generation on Polaroid films.

In liquids with large Raman scattering cross-sections e.g. in CCl_4, CH_3CH_2OH, CH_3CCl_3, CH_3COCH_3, discrete lines were found at $\omega = 2\omega_L + \omega_R$. This light is produced by frequency mixing of two laser quanta and one Raman Stokes quantum. Anti-Stokes light at $\omega = 2\omega_L - \omega_R$ was also found in these substances. Using Equation 22 we find quantitative agreement with the amount of light generated at these wave lengths.

We should emphasize that our investigations on substances other than water are limited; no studies of the resonance structure of $\chi^{(3)}$ were made.

6. Other processes leading to frequency broadening

In this section we briefly discuss other nonlinear processes which are able to produce frequency broadening. Their contribution to our observed broad light spectra is estimated.

6.1. Self-phase modulation

First we discuss the process of self-phase modulation which has been discussed in the literature to explain the super-broadening of picosecond light pulses [1–6, 66, 67]. Self-phase modulation is due to the temporal change of the refractive index [68]. The field of the light pulse may be written in the different forms:

$$\begin{aligned} E(t, z) &= E_0(t, z) \cos(\omega_L t) \\ &= \tilde{E}(t, z) \cos(\omega_L t - kz) = \tilde{E}(t, z) \cos\left[\omega_L \left(t - \frac{n_L}{c} z\right) - \frac{\omega_L z}{c} \Delta n\right] \\ &= \tilde{E}(t', z) \cos\left(\omega_L t' - \frac{\omega_L z}{c} \Delta n\right) \\ &= \tilde{E}(t', z) \cos[-\phi(t', z)] \end{aligned} \tag{32}$$

The relation $k = \omega_L n/c = \omega_L(n_L + \Delta n)/c$ and the transformation $t' = t - n_L z/c$ were used in Equation

32. $\tilde{E}(t', z)$ describes the slowly varying amplitude, ω_L the carrier frequency of the pulse. The instantaneous frequency of the pulse is given by:

$$\omega = -\frac{\partial \phi}{\partial t'} = \omega_L - \frac{\omega_L z}{c}\frac{\partial \Delta n}{\partial t'}. \tag{33}$$

The spectral broadening of the light is found to be

$$\Delta\omega_{br} = \frac{\omega_L z}{c}\left(\left.\frac{\partial \Delta n}{\partial t}\right|_{max} - \left.\frac{\partial \Delta n}{\partial t}\right|_{min}\right) \simeq 2\frac{\omega_L z}{c}\frac{\Delta n}{\Delta t_L}. \tag{34}$$

The change of the refractive index Δn may be caused by (a) the nonlinear polarization at high laser intensities, (b) a laser induced temperature variation, and (c) the generation of free electrons.

6.1.1. Intensity dependent spectral broadening

At high light intensities the refractive index becomes nonlinear and changes proportionally to the square of the light field [68].

$$\Delta n = n_2 \langle E^2(t, z)\rangle = \frac{n_2}{2} E_0^2(t, z). \tag{35}$$

The nonlinear susceptibility $\chi^{(3)}_{xxxx}(-\omega_L; \omega_L, \omega_L, -\omega_L)$ is responsible for the change of the refractive index. The relation between n_2 and $\chi^{(3)}(-\omega_L; \omega_L, \omega_L, -\omega_L)$ is as follows:

$$\begin{aligned} P(t, z) &= \chi_0^{(1)} E(t, z) + \chi_0^{(3)} E^3(t, z) \\ &= \chi_0^{(1)} E(t, z) + 0.25\chi_0^{(3)} E_0^3(t, z)[\cos(3\omega_L t) + 3\cos(\omega_L t)] \\ &= [\chi_0^{(1)} + 0.75\chi_0^{(3)} E_0^2(t, z)] E(t, z). \end{aligned} \tag{36a}$$

$$\begin{aligned} D(t, z) &= E(t, z) + 4\pi P(t, z) \\ &\simeq [1 + 4\pi\chi_0^{(1)} + 3\pi\chi_0^{(3)} E_0^2(t, z)] E(t, z). \end{aligned} \tag{36b}$$

$$\begin{aligned} D(t, z) &= n^2 E(t, z) = (n_L + \Delta n)^2 E(t, z) \\ &\simeq [n_L^2 + n_L n_2 E_0^2(t, z)] E(t, z). \end{aligned} \tag{36c}$$

$$n_L^2 = 1 + 4\pi\chi_0^{(1)} \tag{36d}$$

$$\chi_0^{(3)} = \frac{4}{3}\chi^{(3)}(-\omega_L; \omega_L, \omega_L, -\omega_L). \tag{36e}$$

By comparing Equations 36b and c we find

$$n_2 = \frac{3\pi}{n_L}\chi_0^{(3)} = \frac{4\pi}{n_0}\chi^{(3)}_{xxxx}(-\omega_L; \omega_L, \omega_L, -\omega_L). \tag{37a}$$

Without resonances at ω_L and $2\omega_L$, one has:

$$\chi^{(3)}(-\omega_L, \omega_L, \omega_L, -\omega_L) = 3\chi^{(3)}_{NR}. \tag{37b}$$

In Equation 36a the polarization term proportional to $\cos(3\omega_L t)$ leads to third harmonic generation and does not contribute to self-phase modulation.

The self-phase modulation due to n_2 is a special case of the paramatric four-photon interaction $\omega_1 + \omega_2 \rightarrow \omega_3 + \omega_4$ where the frequencies of the two pump waves and either the signal or the idler wave lie within the bandwidth of the light pulse. In contrast to the parametric four-photon interaction of Section 2.2. the process here has a strong input pulse at the signal or idler wave and does not need to start from quantum noise. The nonlinear susceptibility $\chi^{(3)}_{xxxx}(-\omega_3; \omega_1, \omega_2, -\omega_4)$ is approximately equal to $\chi^{(3)}_{xxxx}(-\omega_L; \omega_L, \omega_L, -\omega_L)$ of Equation 37. The bandwidth of the light pulse is approximately doubled

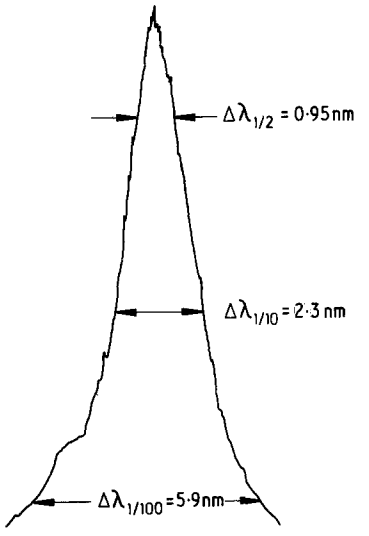

Figure 17 Spectrum of single picosecond laser pulse of $I_{0L} \simeq 2 \times 10^{11}$ W/cm² after passage through a water cell ($l = 2$ cm). The picture shows the microdensitometer trace of a photographic plate.

in each stage of the parametric process $\omega_1 + \omega_2 \rightarrow \omega_3 + \omega_4$ (e.g., for $\omega_L < \omega_1, \omega_2 < \omega_L + \Delta\omega_L/2$) and $\omega_L - \Delta\omega_L/2 < \omega_4 < \omega_L$ signal light is generated at $\omega_L + \Delta\omega_L/2 < \omega_3 < \omega_L + \Delta\omega_L$). For bandwidth limited incident light pulses many stages of parametric processes are necessary to obtain appreciable spectral broadening. On the other side, in parametric four-photon processes starting from quantum noise, $\chi^{(3)}$ may be resonantly enhanced and only one or two stages are necessary to cover the whole visible spectrum. Therefore, the previously discussed four-photon processes (starting from the small quantum noise) readily produce broad light spectra while the spectral broadening due to self-phase

TABLE I Comparison of parametric light generation with self-phase modulation

Substance	Sample length	Shortest wavelength observed (λ_L = 1.06 μm)	Spectral extension	n_2	Self-phase modulation[a]	Self-focusing length[a]
	l (cm)	nm	cm^{-1}	cm³/erg	$\Delta\tilde{\nu}_{br}$ (cm^{-1})	z_f (cm)
H_2O	2	< 200[b]	> 45 000	9×10^{-14}[d]	6	6.4
D_2O	2	< 200[b]	> 45 000			
CH_3CH_2OH	2	≃ 350[c]	≃ 25 000	8×10^{-14}[e]	5	6.8
CCl_4	2	≃ 350[c]	≃ 25 000	1.1×10^{-13}[f]	7	5.8
CH_3CCl_3	2	≃ 350[c]	≃ 25 000			
CH_3COCH_3	2	≃ 350[c]	≃ 25 000	4.3×10^{-13}[g]	28	2.8
CH_2I_2	2	≃ 560[c]	≃ 14 000			
glass BK7	2	≃ 350[c]	≃ 25 000	1.8×10^{-13}[h]	11	4.4
glass SF59	5	≃ 580[c]	≃ 13 000			
quartz glass Suprasil I	2	< 200[b]	> 45 000			
NaCl – crystal	2	< 200[b]	> 45 000	3.2×10^{-13}[i]	19	3.3

[a] Calculated for a laser peak intensity $I_{0L} = 10^{11}$ W/cm², a beam radius of $a = 0.45$ mm (1/e value) and a pulse duration of $\Delta t_L = 6$ ps ($\lambda = 1.06$ μm). Refractive index data are taken from [57].
[b] Measured with double monochromator and photomultiplier.
[c] Measured with spectrograph and Polaroid films.
[d] See [54].
[e] See [88].
[f] Value found with picosecond light pulses ($\lambda = 694.3$ nm) in [89]. For nanosecond light pulses a value of $n_2 = 2 \times 10^{-13}$ cm³/erg was reported [54–56].
[g] See [54–56].
[h] See [87].
[i] See [88].

modulation remains relatively small. On the other hand, with broad input pulses it is certainly possible to generate broad light continua by self-phase modulation. In fact, many authors work with broad-band picosecond input laser pulses ($\Delta\tilde{\nu} \gtrsim 100\,\mathrm{cm}^{-1}$) and obtain the expected super-broad continua.

The spectral broadening by self-phase modulation may be enlarged by the self-steepening of picosecond light pulses [69]. The light pulse forms a very steep tail and $\partial\Delta n/\partial t$ increases. The characteristic length for self-steepening [69] $z_s \simeq 0.19\Delta t_L/(n_2\langle E^2\rangle)$ is estimated to be approximately $z_s \simeq 100\,\mathrm{cm}$ for $\Delta t_L \simeq 6\,\mathrm{ps}$, $I_L = 10^{12}\,\mathrm{W/cm^2}$ and $n_2 \simeq 10^{-13}$ e.s.u. The effect of self-steepening may be neglected in our experiments.

In Table 1, the observed minimum parametric wavelengths, the spectral extension, and the calculated spectral broadening due to self-phase modulation of initially bandwidth limited pulses are listed for several substances ($I_{0L} = 10^{11}\,\mathrm{W/cm^2}$; $\Delta t_L = 6\,\mathrm{ps}$; laser beam radius $a = 0.45\,\mathrm{mm}$ (1/e value)). The data in Table 1 clearly show that the spectral broadening due to self-phase modulation (n_2) is small compared to the observed parametric spectra. The spectrum of a laser pulse of $I_L \simeq 1.5 \times 10^{11}\,\mathrm{W/cm^2}$ transmitted through a water cell of 2 cm length is shown in Fig. 17. The spectrum was measured with a two metre grating spectrograph. On the microdensitometer trace the bandwidths at the intensities 1/2, 1/10, and 1/100 below the peak spectral intensity are shown. Fig. 17 indicates that the main pulse is not broadened substantially down to 1/10 of the peak intensity.

In a recent paper [70], broad band ns-light continua were generated with broad band dye laser pulses ($\Delta\lambda \simeq 15\,\mathrm{nm}$) in Raman active glass fibres. Several high order Stokes Raman components were generated. The spectra were reported to be flattened by self-phase modulation. Here only the primary process $\omega_1 + \omega_2 \rightarrow \omega_3 + \omega_4$ with $\omega_L - \Delta\omega_L/2 \lesssim \omega_1, \omega_2, \omega_3$, or $\omega_4 \lesssim \omega_L + \Delta\omega_L/2$ is necessary to explain the broadening of the laser and Raman spectra. $\chi^{(3)}$ becomes resonantly enhanced by Raman type resonances.

6.1.2. Spectral broadening by thermal effects

When light is absorbed in the medium, the temperature rises and changes the refractive index $n = n_L + (\partial n/\partial T)T$. A corresponding spectral broadening (see Equation 33) has to be considered in absorbing substances and in transparent media with absorbing inclusions.

In absorbing materials the temperature increase during the pulse duration Δt_L is given by:

$$\Delta t = \frac{\partial W}{C\rho\partial V} = \frac{I_{0L}\Delta t_L \alpha \exp(-\alpha z)}{C\rho} \tag{38}$$

where $\partial W/\partial V$ is the absorbed energy per unit volume, C is the heat capacity and ρ the mass density. As a result one estimates for the frequency broadening (see Equation 34 [71]).

$$\Delta\omega_{br} \simeq 2\frac{\omega_L z}{c}\frac{\partial n}{\partial T}\frac{\Delta T}{\Delta t_L} = 2\frac{\omega_L z}{c}\frac{\partial n}{\partial T}\frac{I_{0L}\alpha \exp(-\alpha z)}{C\rho} < 2\frac{\omega_L I_{0L}}{cC\rho}\frac{\partial n}{\partial T}. \tag{39}$$

Similarly, one finds in transparent substances with a large number of absorbing inclusions a spectral increase of [71, 72]:

$$\Delta\omega_{br} \simeq 2\frac{\omega_L}{c}\frac{\partial n}{\partial T}\frac{I_{0L}\epsilon N_i}{C\rho} < 2\frac{\omega_L I_{0L}}{cC\rho}\frac{\partial n}{\partial T}. \tag{40}$$

ϵ is the fraction of light absorbed by one inclusion and N_i is the number of inclusions along the light path. With approximate values of $\partial n/\partial T = 5\times 10^{-5}\,\mathrm{K^{-1}}$ and $C = 1\,\mathrm{J/g \times K}$ we estimate a spectral broadening of $\Delta\nu_{br} = \Delta\omega_{br}/2\pi < 10\,\mathrm{cm}^{-1}$ for $I_{0L} = 10^{12}\,\mathrm{W/cm^2}$. This number strongly suggests that spectral broadening due to the heating of the sample is negligible.

6.1.3. Free electron contribution to spectral broadening

Free electrons generated by multiphoton ionization and avalanche ionization processes change the refractive index according to $n = n_L + \Delta n_p$, where Δn_p is given by:

$$\Delta n_p = \frac{2e^2\tau^2 N_e}{n_L m_e(1+\omega_L^2\tau^2)}. \tag{41}$$

N_e is the density of free electrons with mass m_e. τ is the collision time of the free electrons. The spectral broadening due to Δn_p is approximately:

$$\Delta\omega_{br} \simeq 2\frac{\omega_L z}{c}\frac{2e^2\tau^2 N_e}{n_L m_e(1+\omega_L^2\tau^2)\Delta t_L} \simeq 2\frac{ze^2 N_e}{\omega_L c n_L m_e \Delta t_L}. \tag{42}$$

In the last equation we assumed $\tau \simeq 1/\omega_0$, a good approximation in many cases. From Equation 42 we estimate a spectral broadening of $\Delta\tilde{\nu}_{br} \simeq 200\,\mathrm{cm}^{-1}$ for $N_e = 10^{18}\,\mathrm{cm}^{-3}$. The spectral broadening decreases linearly with the free electron density. At a free electron density of $N_e \simeq 10^{18}\,\mathrm{cm}^{-3}$ damage occurs in the sample [74]. In the pre-breakdown region, at intensities slightly below the damage threshold, the free electron density reduces rapidly.

For the case of multiphoton ionization [75] the electron density is proportional to I_{0L}^n. n is the smallest number of photons necessary to exceed the ionization energy Φ $[(n-1)\hbar\omega_L < \Phi \leqslant n\hbar\omega_L]$ and is of the order of ten. A decrease of the laser intensity by a factor of two decreases the electron density by a factor of $2^n \simeq 10^3$.

In the case of avalanche ionization with picosecond light pulses the electron density is approximately [74]:

$$N_e = N_0 \exp\left\{\int_{-\infty}^{\infty}\eta[I(t)]\,\mathrm{d}t\right\} \simeq N_0 \exp\left[\eta(I)\Delta t_L\right]. \tag{43}$$

In practical situations the initial electron density is $N_0 \simeq 10^7\,\mathrm{cm}^{-3}$ so that $\exp[\eta(I)\Delta t_L] \simeq 10^{11}$ is necessary for damage. Experimental results [76] and theoretical calculations [77, 78] indicate that $\eta(I) \propto I_{0L}$ for picosecond light pulses. A reduction of I_{0L} by a factor 2 below the damage threshold causes a reduction of N_e by a factor of approximately 10^5. These estimates show that spectral broadening due to free electrons can be neglected at intensities below the damage threshold.

The breakdown threshold intensity for H_2O and NaCl has been measured in [71] (see also [79] for measurements on H_2O and [76] for measurements on NaCl). The threshold intensity for plasma formation in water was found to be $I_{0L} \simeq 1.4 \times 10^{13}\,\mathrm{W/cm}^2$ for single picosecond light pulses of 6 ps duration. In NaCl, a damage threshold intensity of $I_{0L} \simeq 1.5 \times 10^{12}\,\mathrm{W/cm}^2$ was measured for the same light pulses.

The high threshold intensities for plasma formation and the rapid reduction of free electrons at intensity values below damage threshold exclude substantial self-phase modulation by free electrons in the intensity range $I_{0L} < 5 \times 10^{11}\,\mathrm{W/cm}^2$, where our experiments of Section 5 were performed.

In a recent paper [80] spectral broadening in KBr crystals could be explained by self-phase modulation due to a large change of refractive index by avalanche ionization. In these experiments self-focusing and filament formation occurred, which favour free electron generation by avalanche ionization.

6.2. Self-focusing

The spatial change of the refractive index within the cross-section of the beam gives rise to catastrophic self-focusing of the laser radiation [68]. Self-focusing of picosecond light pulses increases the light intensity and shortens the pulse duration [81]. The increase of light intensity stimulates nonlinear processes. The shortening of the pulse duration enhances the spectral broadening due to self-phase modulation [66, 67]. The spectral broadening is proportional to $\Delta n/\Delta t_L$ (see Equation 34). Δt_L may become very short ($\Delta t_L \simeq 10^{-13}$ sec) and $\Delta n = n_2 E_0^2/2 + \Delta n_p$ increases rapidly since the laser intensity grows to large values. Plasma formation may set in. In the case of self-focusing, the spectral broadening by self-phase modulation and with the stimulated parametric four-photon light generation contribute both to the formation of broad-band picosecond light spectra.

In our experimental investigations we tried to avoid self-focusing. The self-focusing length z_f was calculated according to the equation [53].

$$z_f = (0.135)^{1/2} ka^2 \{[(P/P_2)^{1/2} - 0.852]^2 - 0.0219\}^{-1/2} \quad (44)$$

where $k = n_L \omega_L / c$ is the wave vector, a is the laser beam radius in the sample (1/e intensity value; in our experiments $a = 0.45$ mm), $P \simeq \pi a^2 \ln(2) I_{0L}$ is the laser power, and $P_2 = 3.72 c^3/(8 n_2 \omega_L^2)$ is the critical self-focusing power.

The self-focusing lengths listed in Table 1 are longer than our sample lengths at a laser intensity of $I_{0L} = 10^{11}$ W/cm^2 ($a = 0.45$ mm, $\lambda_L = 1.06\,\mu$m). At this intensity level, broad light continua were observed in all media (the intensities necessary for rapid growth of parametric light generation range between 1.5×10^{10} W/cm^2 and 4×10^{10} W/cm^2; with the exception of glass SF59 where $I_{0L} \simeq 10^{11}$ W/cm^2 is necessary). Of special interest are the numbers of water. The rapid growth of four-photon parametric light generation starts at 2×10^{10} W/cm^2 in cells of 2 cm length (see Fig. 7). At this intensity value, the self-focusing length is calculated to be $z_f \simeq 16$ cm.

We have calculated the self-focusing length and the parametric four-photon generation for media where $\chi^{(3)}_{NR}$ determines both nonlinear processes (no resonance enhancement of $\chi^{(3)}$, no absorption, small colour dispersion). For high peak intensities $I_{0L} = 10^{11}$ W/cm^2, we find a self-focusing length of $z \simeq 5$ cm and a high gain of $g\chi z = 20$, using the following parameters: $\chi = 3\chi^{(3)}_{NR} = 2 \times 10^{-14}$ cm^3/erg, $z = 2$ cm, $a = 0.45$ mm, $n_L = 1.5$, ($n_L = 1.7 \times 10^{-13}$ e.s.u. is obtained from Equations 37a and b). This estimate shows that even in materials without resonance enhancement large light amplification is possible without self-focusing.

It should be noted that the parametric light generation enlarges the self-focusing length. The new frequencies are emitted into a beam of approximately 4×10^{-2} rad divergence draining energy from the centre of the laser beam.

6.3. Raman scattering

In some substances stimulated Raman scattering [82] converts laser light effectively to other frequency regions at intensities where parametric four-photon processes are still very weak. For instance, in CCl_4, CH_3COCH_3, CH_3CH_2OH, CH_2I_2, and CH_3CCl_3 substantial Stokes intensities were found at $I_{0L} \lesssim 10^{10}$ W/cm^2 (cell length 2 cm), while parametric light was not observed till $I_{0L} \gtrsim 2 \times 10^{10}$ W/cm^2.

In the stimulated Raman process laser photons at ω_L are converted to Stokes photons at ω_S and vibrational phonons at ω_{vib}. The Raman process $\omega_L \rightarrow \omega_S + \omega_{vib}$ is related to the nonlinear coupling term $\chi^{(3)}(-\omega_S; \omega_L, -\omega_L, \omega_S) = \chi'_R + i\chi''_R$. The imaginary part χ''_R determines the efficiency of the Raman scattering, while the real part causes a phase modulation of the Stokes component. χ'_R is zero at $\omega_S = \omega_L - \omega_{vib}$, while χ''_R has its maximum at ω_S. The maximum of the imaginary part is twice the maximum of the real part. There is no phase-mismatch in the Raman scattering. These facts make stimulated Raman scattering $\omega_L + \omega_S \rightarrow \omega_L + \omega_S$ more favourable in strongly Raman active substances than the parametric four-photon process $\omega_L + \omega_L \rightarrow \omega_3 + \omega_4$ (ω_4 around ω_S) of Section 2.2. In these materials parametric four-photon processes start at light intensities higher than necessary for Raman scattering. The generated Raman light as well as the laser light may act as pump wave in the parametric light generation.

The parametric frequency mixing process $\omega_L + \omega_L - \omega_S \rightarrow \omega_{AS}$ of Section 2.4.2. (anti-Stokes light generation) was observed in the substances cited above before the broad band parametric four-photon light generation occurred.

The energy conversion of laser light ($\lambda = 1.06\,\mu$m) into Raman light was found to be small ($\sim 10^{-3}$) for H_2O, D_2O, and Infrasil at $I_{0L} \simeq 2 \times 10^{11}$ W/cm^2 (sample length 2 cm). As shown in Fig. 10, the Raman type resonances do not change $\chi^{(3)}(-\omega_3; \omega_L, \omega_L, -\omega_4)$ substantially and are less important than the infrared resonances in the case of water.

The stimulated Raman scattering in water for picosecond pump pulses at $\lambda = 1.06\,\mu$m may be estimated as follows:

(i) For $I_{0L} \lesssim 10^{11}$ W/cm^2, no Stokes radiation at $\tilde{\nu}_S = \tilde{\nu}_L - \tilde{\nu}_{vib} \simeq 6100$ cm^{-1} is experimentally observed. Using the data for the Raman gain $g_S \simeq 10^{-11}$ cm/W and the Stokes light absorption $\alpha_S = 7$ cm^{-1} one does not expect Stokes light for $I_{0L} \leqslant 7 \times 10^{11}$ W/cm^2, since $I_S(b) = I_S(0)$

$\times \exp[(g_S I_L - \alpha_S)l] < I_S(0)$ [85, 94]. As long as stimulated Stokes light generation does not occur, no strong vibrational field at ω_{vib} is generated and no noticeable anti-Stokes light generation $\omega_L + \omega_{vib} \rightarrow \omega_{AS}$ can take place. Only light generation by parametric four-photon interaction occurs due to the infrared resonances of $\chi^{(3)}$. The parametric light generated at $\omega_3 = \omega_{AS}$ is reduced by inverse Raman scattering $\omega_{AS} \rightarrow \omega_L + \omega_{vib}$ [90]. The reduction of an input signal $\epsilon(\omega_{AS}, 0)$ by inverse Raman scattering is given by:

$$\epsilon(\omega_{AS}, l) = \epsilon(\omega_{AS}, 0) \exp\left[-\frac{n_S \omega_{AS}}{n_{AS} \omega_S} g_S I_L l\right]. \tag{45}$$

For $I_L = 5 \times 10^{10}\,\mathrm{W/cm^2}$ one estimates a loss coefficient of $7\,\mathrm{cm^{-1}}$. This loss factor gives a reduction of parametric light output at $\tilde{\nu}_3 = \tilde{\nu}_{AS} \simeq 12\,900\,\mathrm{cm^{-1}}$ as observed in Fig. 7.

(ii) For $I_{0L} \gtrsim 10^{11}\,\mathrm{W/cm^2}$, Stokes light generation at $\tilde{\nu}_S \simeq 6100\,\mathrm{cm^{-1}}$ was found experimentally; a conversion efficiency of $\eta_S \simeq 10^{-3}$ was observed at $I_{0L} \simeq 2 \times 10^{11}\,\mathrm{W/cm^2}$. Stimulated Stokes generation is expected since the Stokes gain factor $g_S I_L$ exceeds the absorption α_S (see discussion above). The vibrational field generated at ω_{vib} causes some anti-Stokes Raman scattering $\omega_L + \omega_{vib} \rightarrow \omega_{AS}$ which is poorly phase-matched in the forward direction. In addition, the Stokes field generates light at ω_{AS} by parametric four-photon interaction $\omega_L + \omega_L - \omega_S \rightarrow \omega_{AS}$ (Stokes–anti-Stokes coupling). Both processes $\omega_L + \omega_{vib} \rightarrow \omega_{AS}$ and $\omega_L + \omega_L - \omega_S \rightarrow \omega_{AS}$ compensate the loss by inverse Raman scattering $\omega_{AS} \rightarrow \omega_L + \omega_{vib}$ and a rather flat spectral distribution of $\epsilon(\omega_3)$ around $\omega_3 = \omega_{AS}$ is observed (see Fig. 7).

The parametric four-photon interaction in H_2O appears to be influenced by difference frequency resonances when the pump wave is shorter, e.g. at the second harmonic at $\lambda = 0.53\,\mu\mathrm{m}$. In this case the infrared resonances are far away from the pump frequency; i.e. the infrared resonances do not contribute to the parametric light generation at $\tilde{\nu}_S \simeq 16\,600\,\mathrm{cm^{-1}}$. On the other hand, the Stokes gain coefficient is increased by a factor of 2.5 ($g_S(2\omega_L) = [(2\omega_L - \omega_{vib})/(\omega_L - \omega_{vib})] g_S(\omega_L)$) without linear optical absorption at $\omega_S = 2\omega_L - \omega_{vib}$. In fact, considerable Raman Stokes and anti-Stokes light generation was observed experimentally (see also [86, 87]). A detailed study of the build-up of the broad band spectra generated by the second harmonic has not been carried out.

6.4. Contribution from other nonlinear polarization terms

Up to now, the processes discussed were due to the nonlinear polarization term $P_{NL}^{(3)} = \chi_0^{(3)} EEE$. Third order contributions due to magnetic dipole and electric quadrupole interactions are generally small [18, 19] and do not interfere with the generation of picosecond light continua. The second order nonlinear polarization $P_{NL}^{(2)} = \chi_0^{(2)} EE$ is the largest nonlinear term in anisotropic media but it is zero in isotropic and centrosymmetric materials as investigated in this paper. The second order terms resulting from the electric quadrupole and magnetic dipole interactions are small compared to the third order term due to electric dipole interaction and can be neglected. Higher order electric dipole contributions such as $P_{NL}^{(5)} = \chi_0^{(3)} EEEEE$ gain importance at light intensities $I_L > 10^{14}\,\mathrm{W/cm^2}$, which cannot be achieved because of breakdown.

7. Summary

The broad band light generation of intense picosecond light pulses has been studied. It was found that stimulated primary and higher order parametric four-photon processes ($\omega_1 + \omega_2 \rightarrow \omega_3 + \omega_4$) and four-photon frequency conversion ($\omega_1 + \omega_2 + \omega_\gamma \rightarrow \omega$) are responsible for the broad band light generation. In water the absorption of the idler light and the collinear phase-mismatch was overcome by the resonantly enhanced nonlinear susceptibility $\chi^{(3)}$ and the high intensities of the picosecond light pulses. The structure of the spectral distribution of the generated light at moderate laser intensities could be explained by reference to the resonant structure of the nonlinear susceptibility $\chi^{(3)}$. Absolute values of $\chi^{(3)}$ were determined. The flattening of the spectral distribution at high laser intensities results from higher parametric processes and from frequency conversion. It could be shown that other nonlinear broadening mechanisms, such as self-phase modulation, are negligible compared to the parametric

four-photon processes. The parametric four-photon processes remain dominant up to optical breakdown.

Appendix

Relations between fields and intensities in frequency and time domains

In Equation 2, $E(\omega, z)$ (field strength per frequency interval, units e.g. V/cm s^{-1}) is introduced as Fourier transform of the electric field strength $E(t, z)$ (units e.g. V/cm)

$$E(t, z) = (1/2\pi) \int_{-\infty}^{\infty} E(\omega, z) \exp(i\omega t)\, d\omega \tag{A1a}$$

$$E(\omega, z) = \int_{-\infty}^{\infty} E(t, z) \exp(i\omega t)\, dt. \tag{A1b}$$

For these two equations the Parzeval's Equation [89] reads

$$\int_{-\infty}^{\infty} |E(t, z)|^2\, dt = \frac{1}{2\pi} \int_{-\infty}^{\infty} |E(\omega, z)|^2\, d\omega$$

$$= \frac{1}{2\pi} \int_{-\infty}^{\infty} |E_0(\omega, z)|^2\, d\omega. \tag{A2}$$

$E(\omega, z)$ and $E_0(\omega, z)$ are related by $E(\omega, z) = E_0(\omega, z) \exp(-ikz)$. The light intensity $I(t, z)$ (e.g. in W/cm^2) is given by

$$I(t, z) = (cn/4\pi)|E(t, z)|^2.$$

With this relation we rewrite Equation A2

$$\int_{-\infty}^{\infty} I(t, z)\, dt = \frac{cn}{8\pi^2} \int_{-\infty}^{\infty} |E_0(\omega, z)|^2\, d\omega. \tag{A3}$$

Now we define the spectral energy density $\epsilon(\omega, z)$ (e.g. in J/$cm^2 s^{-1}$) by the requirement, that the energy must be the same in time space and in frequency space:

$$\int_{-\infty}^{\infty} I(t, z)\, dt = \int_{-\infty}^{\infty} \epsilon(\omega, z)\, d\omega = \frac{1}{2} \int_{-\infty}^{\infty} \epsilon(\omega, z)\, d\omega. \tag{A4}$$

Comparing Equation A4 with Equation A3 we find for the spectral energy density:

$$\int_{-\infty}^{\infty} \epsilon(\omega, z) = (cn/4\pi^2)|E_0(\omega, z)|^2. \tag{A5}$$

Acknowledgements

The authors are indebted to Dr A. Laubereau for many helpful discussions. They wish to thank A. Seilmeier and W. Falkenstein for skilful assistance during part of the experiments.

References

1. R. R. ALFANO and S. L. SHAPIRO, *Phys. Rev. Lett.* **24** (1970) 592–4.
2. *Idem, ibid* **24** (1970) 584–7.
3. N. G. BONDARENKO, I. V. EREMINA, and V. I. TALANOV, *Sov. Phys. Jetp-Lett.* **12** (1970) 85–7.
4. N. N. IL'ICHEV, V. V. KOROBKIN, V. A. KORSHUNOV, A. A. MALYUTIN, T. G. OKROASKVILI, and P. P. PASHININ, *ibid* **15** (1972) 133–5.
5. W. WERNCKE, A. LAU, M. PFEIFFER, K. LENZ, H. J. WEIGMANN, and C. D. THUY, *Opt. Commun.* **4** (1972) 413–5.
6. G. E. BUSCH, R. P. JONES and P. M. RENTZEPIS, *Chem. Phys. Lett.* **18** (1973) 178–85.
7. D. K. SHARMA, R. W. YIP, D. F. WILLIAMS, S. E. SUGAMORY and L. L. T. BRADLEY, *ibid* **41** (1976) 460–5.
8. A. PENZKOFER, A. LAUBEREAU and W. KAISER, *Phys. Rev. Lett.* **31** (1973) 863–6.

9. A. P. VEDUTA, N. B. FEDOTOV and N. P. FURZIKOV, *Sov. Phys. Jetp-Lett.* **16** (1972) 281–4.
10. D. MADGE and M. W. WINDSOR, *Chem. Phys. Lett.* **27** (1974) 31–6.
11. H. TASHIRO and T. YAJIMA, *ibid* **25** (1974) 582–6; R. M. HOCHSTRASSER, D. S. KING and A. C. NELSON, *ibid* **42** (1976) 8–12.
12. P. M. RENTZEPIS, R. P. JONES and J. JORTNER, *J. Chem. Phys.* **59** (1973) 766–73.
13. H. KURODA and S. SHIONOYA, *Sol. State Commun.* **13** (1973) 1195–6;
14. *Idem, Opt. Commun.* **10** (1974) 74–7.
15. A. PENZKOFER, W. FALKENSTEIN and W. KAISER, *Appl. Phys. Lett.* **28** (1976) 319–21.
16. J. A. ARMSTRONG, N. BLOEMBERGEN, J. DUCUING and P. S. PERSHAN, *Phys. Rev.* **127** (1962) 1918–39.
17. N. BLOEMBERGEN, 'Nonlinear Optics', (Benjamin, New York, 1965).
18. R. W. TERHUNE and P. D. MAKER, 'Lasers', Vol. 2, Ch. 4 Edited by A. K. Levine, (Marcel Dekker, New York, 1968).
19. P. D. MAKER and R. W. TERHUNE, *Phys. Rev.* **137** (1965) A801–18.
20. H. PAUL, 'Nichtlineare Optik', Vol. 1 and 2, (Akademie-Verlag, Berlin, 1973).
21. C. FLYTZANIS, 'Quantum Electronics', Vol. 1, Ch. 2, Edited by H. Rabin and C. L. Tang, (Academic Press, New York, 1975).
22. G. C. BJORKLUND, *IEEE J. Quant. Elec.* **QE-11** (1975) 287–96.
23. A. YARIV, 'Quantum Electronics', (Wiley, New York, 1968).
24. J. P. GORDON, W. H. LOUISELL and L. R. WALKER, *Phys. Rev.* **129** (1963) 481–5.
25. V. R. SHEN, *Phys. Rev.* **155** (1967) 921–31.
26. D. A. KLEINMAN, *ibid* **174** (1968) 1027–41.
27. W. H. LOUISELL, 'Quantum Statistical Properties of Radiation', (J. Wiley & Sons, New York, 1973).
28. A. PENZKOFER, A. SEILMEIER and W. KAISER, *Opt. Commun.* **14** (1975) 363–7.
29. E. A. STAPPAERTS, G. W. BEKKERS, J. F. YOUNG and S. E. HARRIS, *IEEE J. Quant. Elec.* **QE-12** (1976), 330–3.
30. R. T. HODGSON, P. P. SOROKIN and J. J. WYNNE, *Phys. Rev. Lett.* **32** (1974) 343–6.
31. C. WALLACE, C. H. LEE and W. L. FAUST, *Opt. Commun.* **18** (1976) 110–1.
32. R. T. ROYT, C. H. LEE and W. L. FAUST, *ibid.* **18** (1976) 108–9.
33. M. D. LEVENSON, C. FLYTZANIS and N. BLOEMBERGEN, *Phys. Rev.* **B6** (1972) 3962–5.
34. J. J. WYNNE, *Phys. Rev. Lett.* **29** (1972) 650–3.
35. M. D. LEVENSON and N. BLOEMBERGEN, *Phys. Rev.* **B10** (1974) 4447–63.
36. P. R. REGNIER, F. MOYA and J. P. E. TARAN, *AIAA J.* **12** (1973) 826–31.
37. R. F. BEYLEY, A. B. HARVEY and R. L. BYER, *Appl. Phys. Lett.* **25** (1974) 387–90.
38. I. ITZKAN and D. A. LEONARD, *ibid* **26** (1975) 106–8.
39. R. B. MILES and S. E. HARRIS, *IEEE J. Quant. Elec.* **QE-9** (1973) 470–84.
40. K. M. LUNG, J. F. WARD and B. J. ORR, *Phys. Rev.* **A9** (1974) 2440–8.
41. H. PUELL, C. R. VIDAL, K. SPANNER, W. FALKENSTEIN and W. KAISER, *Phys. Rev.* **A14** (1976) 2240–57.
42. R. H. PANTELL and H. E. PUTHOFF, 'Fundamentals of Quantum Electronics', (J. Wiley & Sons, New York, 1969).
43. P. D. MAKER, R. W. TERHUNE and C. M. SAVAGE, *Phys. Rev. Lett.* **12** (1964) 507–9.
44. J. DAVIT, National Bureau of Standards Special Publication **341** (1970) 37–44.
45. A. OWYOUNG, *Opt. Commun.* **16** (1976) 266–271.
46. D. MILAM and M. J. WEBER, *J. Appl. Phys.* **47** (1976) 2497–501.
47. D. VON DER LINDE, *IEEE J. Quant. Elec.* **QE-8** (1972) 328–38.
48. A. LAUBEREAU and W. KAISER, *Opto-Electronics* **6** (1974) 1–24.
49. D. VON DER LINDE, O. BERNECKER and A. LAUBEREAU, *Opt. Commun.* **2** (1970) 215–8.
50. A. PENZKOFER, D. VON DER LINDE and A. LAUBEREAU, *Opt. Commun.* **4** (1972) 377–9.
51. G. BRET and B. MAYER, 'Physics of Quantum Electronics', Edited by P. L. Kelley, B. Lax and P.E. Tannenwald, (McGraw-Hill, New York, 1966) p. 180–191.
52. O. RAHN, M. MAIER and W. KAISER, *Opt. Commun.* **1** (1969) 109–10.
53. J. M. MARBURGER, *Prog. Quant. Elect.* **4** (1975) 35–110.
54. M. PAILLETTE, *Ann. Phys. (Paris)* **4** (1969) 671–712.
55. P. D. MCWANE and D. A. SEALER, *Appl. Phys. Lett.* **8** (1966) 278–9.
56. F. SHIMIZU, *J. Phys. Soc. Japan* **22** (1967) 1070–7.
57. LANDOLT-BÖRNSTEIN, 6th Edition, Vol. 2, Part 8, (Springer-Verlag, Berlin, 1962).
58. E. K. PLYLER and N. ACQUISTA, *J. Opt. Soc. Amer.* **44** (1954) 505.
59. N. E. DORSEY, 'Properties of Ordinary Water-Substance', (Reinhold, New York, 1940).
60. D. L. WEINBERG, *Appl. Phys. Lett.* **14** (1969) 32–34.
61. M. BECKER, R. FISCHER, J. FRAHM, R. GÜTHER and J. STREUDEL, *Opt. Quant. Elect.* **8** (1976) 279–84.
62. P. P. SOROKIN, J. J. WYNNE and J. R. LANKARD, *Appl. Phys. Lett.* **22** (1973) 342–4.

63. P. P. SOROKIN, *Opt. Commun.* **18** (1976) 110.
64. R. FREY, F. PRADERE and J. DUCUING, *Opt. Commun.* **18** (1976) 204.
65. J. PETRUSKA, *J. Chem. Phys.* **34** (1961) 1120–36.
66. R. R. ALFANO, L. L. HOPE and S. L. SHAPIRO, *Phys. Rev.* **A6** (1972) 433–8.
67. R. R. ALFANO, J. I. GERSTEN, G. A. ZAWADZKAS, and N. TZOAR, *ibid* **A10** (1974) 698–708.
68. S. A. AKHMANOV, R. V. KHOKHLOV and A. P. SUKHORUKOV, 'Laser Handbook', Vol. 2, Ch. E3, Edited by F. T. Arecchi and E. O. Schulz-Dubois, (North-Holland, Amsterdam, 1972).
69. F. DEMARTINI, C. H. TOWNES, T. K. GUSTAFSON and P. L. KELLEY, *Phys. Rev.* **164** (1967) 312–23.
70. C. LIN and R. H. STOLEN, *Appl. Phys. Lett.* **28** (1976) 216–8.
71. A. PENZKOFER, *Opt. Commun.* **11** (1974) 265–9.
72. R. W. HOPPER and D. R. UHLMANN, *J. Appl. Phys.* **41** (1970) 4023–37.
73. N. BLOEMBERGEN, *Opt. Commun.* 8 (1973) 285–8.
74. N. BLOEMBERGEN, *IEEE J. Quant. Elect.* **QE-10** (1974) 375–86.
75. L. V. KELDYSH, *Sov. Phys. Jetp* **20** (1965) 1307–14.
76. D. W. FRADIN, N. BLOEMBERGEN and I. P. LETELLIER, *Appl. Phys. Lett.* **22** (1973) 635–7.
77. M. BASS and H. H. BARRETT, *IEEE J. Quant. Elect.* **QE-8** (1972) 338–43.
78. L. H. HOLWAY, *Phys. Rev. Lett.* **28** (1972) 280–3.
79. R. YU. ORLOW, I. B. SKIDAN, and L. S. TELEGIN, *Sov. Phys. Jetp* **34** (1972) 418–21.
80. W. YU, R. R. ALFANO, C. L. SAM and R. J. SEYMOUR, *Opt. Commun.* **14** (1975) 344–7.
81. F. SHIMIZU, *IBM J. Res. Dev.* **17** (1973) 286–98.
82. W. KAISER and M. MAIER, 'Laser Handbook', Vol. 2, Ch. E2, Edited by F. T. Arecchi and E. O. Schulz-Dubois, (North-Holland, Amsterdam, 1972).
83. C. A. G. O. VARMA and P. M. RENTZEPIS, *Chem. Phys. Lett.* **19** (1973) 162–5.
84. M. SCEATS, S. A. RICE and J. E. BUTLER, *J. Chem. Phys.* **63** (1975) 5390–400.
85. Y. R. SHEN, *Phys. Lett.* **20** (1966) 378–80.
86. R. HELLWARTH, A. OWYOUNG and N. GEORGE, *Phys. Rev.* **A4** (1971) 2342–47.
87. M. A. DUGUAY, J. W. HANSEN and S. L. SHAPIRO, *IEEE J. Quant. Elect.* **QE-6** (1970) 725–43.
88. C. C. WANG, *Phys. Rev.* **B2** (1970) 2045.
89. A. PAPOULIS, 'The Fourier Integral and its Applications', (McGraw-Hill, New York, 1962).
90. W. J. JONES and B. P. STOICHEFF, *Phys. Rev. Lett.* **13** (1964) 657–9.